THE JOURNAL OF BIOLOGICAL CHEMISTRY VOL. 281, NO. 24, pp. 16768–16776, June 16, 2006

Differential Metabolomics Reveals Ophthalmic Acid as an Oxidative Stress Biomarker Indicating Hepatic Glutathione Consumption*[S]

Received for publication, February 27, 2006, and in revised form, March 29, 2006 Published, JBC Papers in Press, April 11, 2006, DOI 10.1074/jbc.M601876200

Tomoyoshi Soga[‡§1,2], **Richard Baran**[‡1], **Makoto Suematsu**[¶1,3], **Yuki Ueno**[‡§], **Satsuki Ikeda**[‡], **Tadayuki Sakurakawa**[¶], **Yuji Kakazu**[‡], **Takamasa Ishikawa**[§], **Martin Robert**[‡], **Takaaki Nishioka**[‡], **and Masaru Tomita**[‡§]

From the [‡]Institute for Advanced Biosciences, Keio University, Tsuruoka, Yamagata 997-0017, Japan, [§]Human Metabolome Technologies Inc., Tsuruoka, Yamagata 997-0017, Japan, and the [¶]Department of Biochemistry and Integrative Medical Biology, School of Medicine, Keio University, Shinanomachi, Shinjuku-ku, Tokyo 160-8582, Japan

Metabolomics is an emerging tool that can be used to gain insights into cellular and physiological responses. Here we present a metabolome differential display method based on capillary electrophoresis time-of-flight mass spectrometry to profile liver metabolites following acetaminophen-induced hepatotoxicity. We globally detected 1,859 peaks in mouse liver extracts and highlighted multiple changes in metabolite levels, including an activation of the ophthalmate biosynthesis pathway. We confirmed that ophthalmate was synthesized from 2-aminobutyrate through consecutive reactions with γ-glutamylcysteine and glutathione synthetase. Changes in ophthalmate level in mouse serum and liver extracts were closely correlated and ophthalmate levels increased significantly in conjunction with glutathione consumption. Overall, our results provide a broad picture of hepatic metabolite changes following acetaminophen treatment. In addition, we specifically found that serum ophthalmate is a sensitive indicator of hepatic GSH depletion, and may be a new biomarker for oxidative stress. Our method can thus pinpoint specific metabolite changes and provide insights into the perturbation of metabolic pathways on a large scale and serve as a powerful new tool for discovering low molecular weight biomarkers.

An excess dose of acetaminophen (AAP),[4] the most commonly used analgesic, can lead to possibly fatal hepatitis and more than 100 such deaths occur in the United States annually. AAP is normally detoxified by sulfation or glucoronidation followed by elimination (1). In high doses, it is metabolized by P450 cytochromes to generate the reactive intermediate *N*-acetyl-*p*-benzoquinone imine (NAPQI) (2), which is further inactivated by conjugation with glutathione (GSH) before excretion. This results in a sudden drop in GSH levels (3). In absence of sufficient GSH, the reactive NAPQI can cause toxic and covalent protein modifications that lead to cell death and tissue injury (4–7).

Recent transcriptomic and proteomic studies showed that AAP can cause numerous changes in gene and protein expression levels in pathways related to cellular stress response, mitochondrial function, and metabolism, as well as in cell cycle, structural, signaling, and apoptotic proteins (8, 9). However, little is known about global changes in metabolites. Global information about when and where metabolite levels increase or decrease can reveal connections in biological networks and provide a system level understanding of the cell (10–14). However, unlike other functional genomic approaches, metabolome analysis methods are still under development. Current large scale metabolite analysis methods are based on gas chromatography mass spectrometry (15), liquid chromatography mass spectrometry (LC-MS) (16), NMR (17), Fourier transform ion cyclotron resonance mass spectrometry) (18), and capillary electrophoresis mass spectrometry (CE-MS) (19). Whereas these analytical tools allow global metabolite profiling, the exploration and identification of changes in compounds among the enormous amount of data generated are laborious.

Here, we propose a novel strategy to analyze and differentially display metabolic profiles by coupling capillary electrophoresis with electrospray ionization time-of-flight mass spectrometry (CE-TOFMS). Using this profiling system, we determined global changes in metabolite levels in the liver and serum of AAP-treated mice, obtained insights into the perturbation of metabolic pathways related to hepatotoxicity, and identified biomarkers that can reveal acute liver injury.

MATERIALS AND METHODS

Animals and Drug Administration—Male C57BL6 mice, fasted overnight with free access to water, were anesthetized with an intraperitoneal (ip) injection of pentobarbital sodium (60 mg/kg). AAP or physiological saline as a vehicle was administered at 150 mg/kg. AAP was solubilized in saline prior to injection, to avoid the use of ethanol that could affect liver function. To achieve solubilization, AAP was added to warm saline kept at 42 °C followed by vortexing for 1 h. After the AAP injection, mice were allowed free access to chow diet and water. At the indicated times after AAP administration (1, 2, 4, 6, 12, and 24 h) the mice were anesthetized by urethane and were sacrificed to collect liver tissues and serum samples. The liver tissues were immediately snap-frozen in liquid nitrogen (20). In another set of experiments, diethylmaleate (DEM) or buthionine sulfoximine (BSO) (4 mmol/kg) was administered ip while the control mice were injected with physiological saline.

* This work was supported in part by a grant from the Ministry of Education, Culture, Sports, Science, and Technology (MEXT) (the 21st Century COE Program entitled "Understanding and Control of Life's Function via Systems Biology," and a grant from Grant-in-aid of Creative Researches and Leading Project for Biosimulation from MEXT in Japan as well as research funds from Yamagata prefectural government and Tsuruoka city. The costs of publication of this article were defrayed in part by the payment of page charges. This article must therefore be hereby marked "*advertisement*" in accordance with 18 U.S.C. Section 1734 solely to indicate this fact.

[S] The on-line version of this article (available at http://www.jbc.org) contains supplemental data.

[1] These authors contributed equally to this work.

[2] To whom correspondence may be addressed: Institute for Advanced Biosciences, Keio University, Tsuruoka, Yamagata 997-0017, Japan. Tel.: 81-235-29-0528; Fax: 81-0235-29-0530; E-mail: soga@sfc.keio.ac.jp.

[3] To whom correspondence may be addressed: Dept. of Biochemistry and Integrative Medical Biology, School of Medicine, Keio University, Shinanomachi, Shinjuku-ku, Tokyo 160-8582, Japan. E-mail: msuem@sc.itc.keio.ac.jp.

[4] The abbreviations used are: AAP, acetaminophen; CE-TOFMS, capillary electrophoresis time-of-flight mass spectrometry; 2AB, 2-aminobutyrate; GCS, γ-glutamylcysteine synthetase; GS, glutathione synthetase; ip, intraperitoneal; DEM, diethylmaleate; BSO, buthionine sulfoximine; MES, 2-morpholinoethanesulfonate; Oct RFV, octapole radio frequency voltage; ESI-Q-TOFMS, electrospray ionization quadrupole time-of-flight mass spectrometry; PIPES, piperazine-1,4-bis(2-ethansulfonate).

At the above time points post-administration, livers and serum samples were collected for metabolome analysis.

Metabolite Extraction—Frozen liver tissue (~300 mg) was immediately plunged into methanol (1 ml) containing internal standards (300 μM each of methionine sulfone for cations, MES for anions) and homogenized for 1 min to inactivate enzymes. Then, deionized water (500 μl) was added, 300 μl of the solution were transferred to another tube, and 200 μl of chloroform were added, and the mixture thoroughly mixed. The solution was centrifuged at 12,000 × *g* for 15 min at 4 °C, and the 300-μl upper aqueous layer was centrifugally filtered through a Millipore 5-kDa cutoff filter to remove proteins. The filtrate was lyophilized and dissolved in 50 μl of Milli-Q water containing reference compounds (200 μM each of 3-aminopyrrolidine and trimesate) prior to CE-TOFMS analysis.

For serum studies, 200-μl samples were plunged into 1.8 ml of methanol containing 55 μM each of methionine sulfone and MES and mixed well. Then 800 μl of deionized water and 2 ml of chloroform were added, and the solution was centrifuged at 2,500 × *g* for 5 min at 4 °C. The 800-μl upper aqueous layer was centrifugally filtered through a Millipore 5-kDa cutoff filter to remove proteins. Subsequent steps were as for liver samples.

Metabolite Standards—All chemical standards were obtained from common commercial sources and dissolved in Milli-Q (Millipore, Bedford, MA) water, 0.1 N HCl or 0.1 N NaOH to obtain 10 mM or 100 mM stock solutions. Working standard mixtures were prepared by diluting stock solutions with Milli-Q water just prior to injection into the CE-TOFMS. The chemicals used were of analytical or reagent grade.

Instrumentation—All CE-TOFMS experiments were performed using an Agilent CE capillary electrophoresis system (Agilent Technologies, Waldbronn, Germany), an Agilent G3250AA LC/MSD TOF system (Agilent Technologies, Palo Alto, CA), an Agilent1100 series binary HPLC pump, and the G1603A Agilent CE-MS adapter and G1607A Agilent CE-ESI-MS sprayer kit. For system control and data acquisition we used the G2201AA Agilent ChemStation software for CE and the Analyst QS for Agilent TOFMS software. CE-MS/MS analyses for compound identification were performed on a Q-Star XL Hybrid LC-MS/MS System (Applied Biosystems, Foster City, CA) connected to an Agilent CE instrument.

CE-TOFMS Conditions for Cationic Metabolite Analysis—Separations were carried out in a fused silica capillary (50 μm inner diameter × 100 cm total length) filled with 1 M formic acid as the electrolyte (21). Approximately 3 nl of sample solution were injected at 50 mbar for 3 s, and 30 kV of voltage was applied. The capillary temperature was maintained at 20 °C, and the sample tray was cooled below 5 °C. Methanol-water (50% v/v) containing 0.5 μM reserpine was delivered as the sheath liquid at 10 μl/min. ESI-TOFMS was operated in the positive ion mode, and the capillary voltage was set at 4,000 V. A flow rate of heated dry nitrogen gas (heater temperature 300 °C) was maintained at 10 psig. In TOFMS, the fragmentor, skimmer, and Oct RFV voltage were set at 75 V, 50 V, and 125 V, respectively. Automatic recalibration of each acquired spectrum was performed using reference masses of reference standards. The methanol adduct ion ($[2MeOH + H_2O + H]^+$, *m/z* 83.0703) and reserpine ($[M + H]^+$, *m/z* 609.2806) provided the lock mass for exact mass measurements. Exact mass data were acquired at a rate of 10 spectra/s over a 50–1,000 *m/z* range.

CE-TOFMS Conditions for Anionic Metabolite Analysis—A cationic polymer-coated SMILE (+) capillary (22) (Nacalai Tesque, Kyoto, Japan) was used as the separation capillary (23). A 50 mM ammonium acetate solution (pH 8.5) was used as electrolyte solution for CE separation. Sample solution (30 nl) was injected at 50 mbar for 30 s and −30 kV of voltage was applied. Ammonium acetate (5 mM) in 50% methanol-water (v/v) containing 20 μM PIPES and 1 μM reserpine was delivered as the sheath liquid at 10 μl/min. ESI-TOFMS was conducted in the negative ion mode; the capillary voltage was set at 3,500 V. For TOFMS, the fragmentor, skimmer, and Oct RFV voltage were set at 100 V, 50 V, and 200 V, respectively. Automatic recalibration of each acquired spectrum was performed using reference masses of standards, i.e. divalent PIPES ($[M - 2H]^{2-}$, *m/z* 150.0230), monovalent PIPES ($[M - H]^-$, *m/z* 301.0534), and reserpine ($[M - H]^-$, *m/z* 607.2661). Other conditions were identical to those used in cationic metabolite analysis.

CE-Q-TOFMS Conditions for the Acquisition of MS/MS Spectra—Most of the conditions were identical to those in cationic metabolite analysis using CE-TOFMS. Methanol-water (50% v/v) containing 1 μM reserpine was delivered as the sheath liquid at 5 μl/min. ESI-Q-TOFMS was conducted in the positive product ion scan mode; the ion spray voltage was set at 5,500V. Dry air (GS1) was maintained at 10 psi. The declustering potential 1 and 2, and the collision energy voltage were set at 60 V, 15 V, and 20 V, respectively. Recalibration was manually performed with reserpine ($[M + H]^+$, *m/z* 609.2806) and its fragment ion ($[M + H]^+$, *m/z* 195.0652).

Data Processing for the Generation of the Metabolome Differential Display—Raw datasets were preprocessed by binning the data along the *m/z* axis to 0.02 *m/z* resolution, subtracting the baseline from each electropherogram by robust nonlinear fitting of the data to a 7th order polynomial and removing the noise from each electropherogram by leveling to 0 all signal intensity values that fell within 5× S.D. of the signal intensities from 1 to 4 min. The resulting data sets were then further binned to 1 *m/z* unit resolution along the *m/z* axis. A set of peaks was selected from each dataset using a modified Douglas-Peucker algorithm (24); alignment of datasets along the migration time axis was as described in the text. Annotation tables for both cation and anion modes were generated based on the results of the CE-TOFMS analysis of standard compounds. The annotation labels were aligned to the actual datasets in a similar fashion. Arithmetic operations were applied to whole datasets on a data point-by-data point basis to highlight differences of interest. Averaging the datasets within each group allowed visualization of absolute (difference between the corresponding intensities from the averaged datasets) and relative (absolute difference divided by the larger of the two corresponding intensities) differences. To generate the metabolome differential displays shown in Fig. 1 and supplemental Fig. S1, the product of two results was used so that differences significant in both absolute and relative terms were preferentially visualized. Overlaid electropherograms in the vicinity of the most significant differences from the results of interest were plotted in descending order of significance for visual confirmation. A Mathematica (Wolfram Research Inc.) package for differential analysis of metabolite profiles, a detailed description of which is beyond the scope of this manuscript, will be released separately.

RESULTS AND DISCUSSION

Development of Metabolome Differential Display—By coupling a CE system with an Agilent TOFMS instrument, we developed a new analytical system for metabolome differential display. Because TOFMS instruments are usually calibrated to analyze macromolecules like peptides and proteins, we first optimized the settings of the ion guide optics, i.e. the fragmentor, skimmer, and Oct RFV voltage for the analysis of low molecular mass substances (50–1,000 Da). This optimization enabled the sensitive detection of small molecules. To measure the system's reliability, we then analyzed 338 cations by CE-TOFMS and measured the errors in mass accuracy. These errors were nonlinearly related to the *m/z* values and were less than 10 ppm in the range from 200 to 400 *m/z* and less than 30 ppm outside this range (see Fig. 2*A*). Because errors in

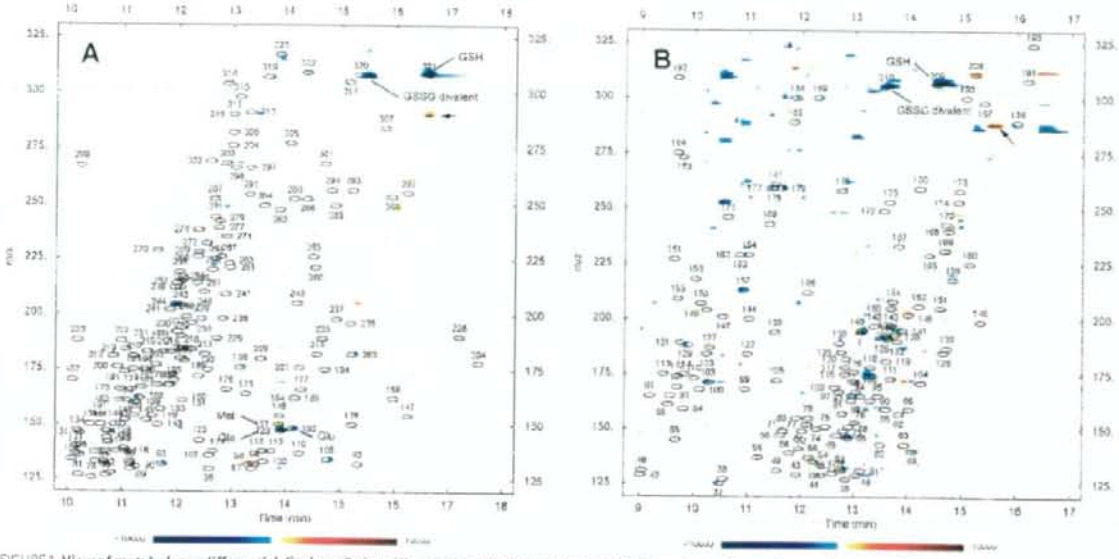

FIGURE 1. **View of metabolome differential displays.** Cations (*A*) and anions (*B*) obtained from CE-TOFMS analyses of livers of control mice ($n = 5$) and mice 2 h after intraperitoneal injection with AAP ($n = 5$). The plots were generated as described under "Materials and Methods," and the position of standard compounds is overlaid with the differential profiles and numbers correspond to compounds listed in supplemental Table S2. The *arrow* points to the metabolite (later identified as ophthalmate) whose level significantly increased ($p < 0.05$) in AAP-treated mice. Anion peaks 208, 209, and 210 on *plot B* were identified by CE-TOFMS as mercapturate, GSH, and GSSG divalent ion. The gradation of the color bar indicates the increase (*red*) or the decrease (*blue*) of the metabolite level after AAP administration.

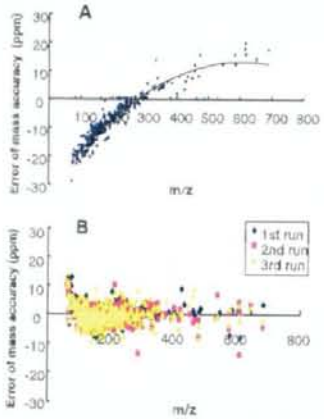

FIGURE 2. **Mass accuracy for triplicate measurements of a mixture of 338 cations (20 μM each) obtained by CE-TOFMS.** *A*, standard mass calibration before analysis or *B*, real-time recalibration for every mass spectrum using the sheath liquid calibrant method (*blue*, *magenta*, and *yellow* colors indicate the results obtained by 1st, 2nd, and 3rd run, respectively).

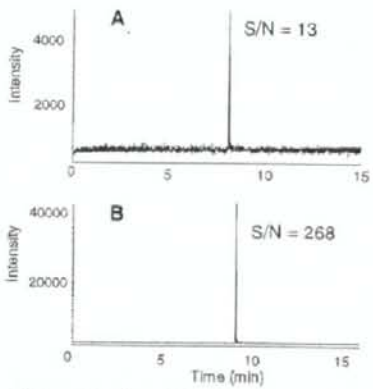

FIGURE 3. **CE-TOFMS sensitivity for arginine (10 μM).** *A*, the reference sprayer recalibration (signal-to-noise ratio, S/N = 13) and *B*, the sheath liquid recalibration method (S/N = 268) are shown.

TOFMS measurements seemed to be attributed to real time fluctuations in environmental conditions such as temperature and vacuum, we opted to constantly deliver a calibrant solution using a reference sprayer (second sprayer) provided with the Agilent TOFMS system, and recalibrated the mass axis for each spectrum using the measurement of known reference masses (*i.e.* "lock masses") (25). Although this lock-mass spray improved the mass accuracy, detection sensitivity decreased considerably (Fig. 3*A*). We believe that this decrease in sensitivity may be because of interference by the reference sprayer and/or to dilution of analyte solution (several μl/min) in the calibrant solution (100 μl/min).

To overcome this problem, we added reserpine (mass recalibration standard) directly to the sheath solution, used to assist electrospray ionization (flow rate 10 μl/min). In addition to the spiked reserpine standard ($[M + H]^+$, *m/z* 609.2806) the methanol adduct ion ($[2MeOH + H_2O + H]^+$, *m/z* 83.0730) found in the sheath solution was also used as another calibrant. This procedure provided mass accuracies within 10 ppm for almost all compounds (Fig. 2*B*) and a more than 20-fold increase in sensitivity (Fig. 3*B*). Similarly, we recalibrated the mass accuracy for anionic compounds using a sheath liquid containing three calibrants, *i.e.* divalent PIPES ($[M - 2H]^{2-}$, *m/z* 150.0230), monovalent PIPES ($[M - H]^-$, *m/z* 301.0534), and reserpine ($[M - H]^-$, *m/z* 607.2661), yielding satisfactory results (data not shown).

Next, we validated the CE-TOFMS methods using amino acids or phosphorylated compounds as representatives of cationic and anionic metabolites, respectively. Good reproducibility, linearity, and sensitivity were obtained (see supplemental Table S1). Specially, the detection lim-

its for most amino acids and anionic species in CE-TOFMS were improved on average severalfold and as much as 65-fold over previously reported values for the CE-quadrupole mass spectrometer (QMS) (21, 23). We attribute this significant increase in sensitivity to the fact that TOFMS allows more ions to reach the detector during the instrument duty cycle and that the exact mass resolution of the TOF instrument results in a considerable reduction in the baseline noise.

To facilitate the analysis and comparison of large and complex data sets produced by CE-MS analysis, visualization tools are desirable. Few available tools exist to do this, especially for CE-MS data where migration time variations between samples are significant. An important issue in the development of a differential displays tool is thus the normalization of the compound migration times. The function derived by Reijenga *et al.* (26) for electropherogram normalization in CE fit the shifts in migration times between corresponding peaks from different data sets. To align the peaks from two CE-MS data sets, the sum of dynamic programming (DP) scores, serving as a measure of the quality of the alignment, was calculated for all corresponding electropherograms. Partial scores (or gap penalty values) were assigned to the distance between two peaks of a subproblem and the Reijenga function parameters were optimized to achieve the lowest overall DP score (Fig. 4). The time scale of the sample data set was then rescaled to that of the reference and signal intensities were adjusted accordingly to compensate for the compression or expansion of the peaks, thereby conserving their original peak areas.

Differential Display of Liver Metabolites in Acetaminophen-treated Mice—To evaluate the power of our metabolite profiling and differential display methods to pin-point changes in the metabolome in an unbiased manner and identify biomarkers, we determined the changes in murine hepatic metabolite levels after AAP administration. To facilitate the assignment of specific metabolites to peaks, we first analyzed 569 metabolic standards listed in the KEGG LIGAND data base (27) by CE-TOFMS before analyzing tissue-derived samples. Global mass scanning over a 50–1,000 *m/z* range was applied in both cation and anion CE modes. Almost all compounds were well resolved and were annotated with numbers referring to the compound list (supplemental Fig. S1, *A* and *B* and supplemental Table S2). To study the effects of AAP on liver metabolism, we determined liver metabolite levels two hours (control, supplemental Fig. S1, *C* and *D*) after injection with either saline or AAP (point where liver damage is maximum, supplemental Fig. S1, *E* and *F*). Our metabolome differential data analysis tool automatically normalized the migration times of all peaks in the samples and matched these with the standard annotation table. This allowed to readily identify the corresponding peaks. A total of 132 metabolites were identified among 1,859 detected peaks (supplemental Table S3).

Among the several changes, differential display of liver metabolites between the controls and AAP treated (2 h) showed extensive depletion of GSH and its oxidized form (GSSG), detected as a divalent ion (Fig. 1). In paired Student's *t* tests, the level of 13 identifiable metabolites were significantly different ($p < 0.01$), and most were part of metabolic processes proximal to glutathione biosynthesis such as the transsulfuration pathway, taurine shunt, and remethylation cycles (supplemental Table S3). As seen when plotting results on the glutathione biosynthesis pathways (Fig. 5*A*), the level of most of these metabolites decreased at 2-h post-AAP treatment. These metabolite changes are likely linked to the GSH depletion by conjugation (oxidation) with NAPQI, and the associated depletion of intermediates for glutathione biosynthesis. On the other hand, the level of methionine, an essential amino acid located upstream in the cysteine synthesis pathway, more than doubled in AAP-treated mice. This alteration could be the result of the AAP-elicited

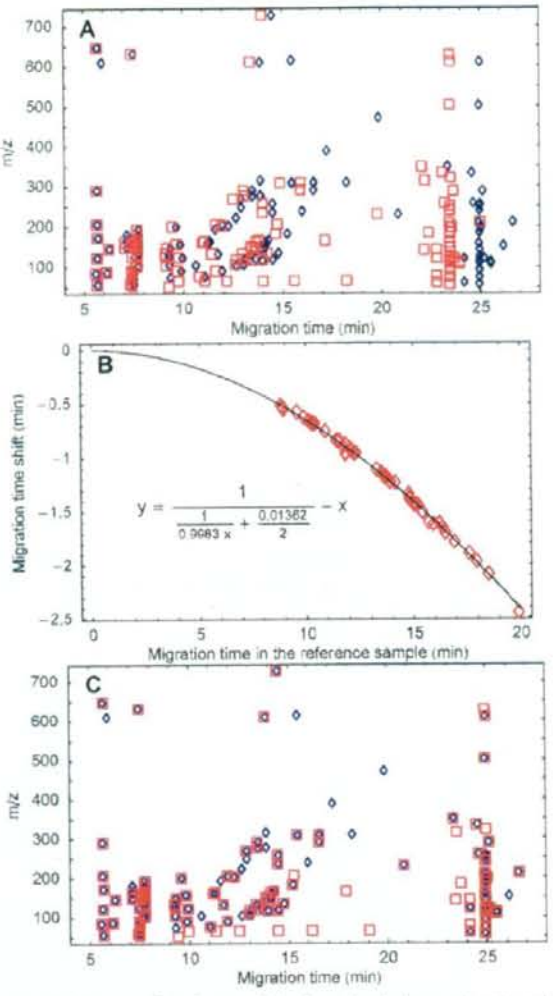

FIGURE 4. **Alignment of two datasets.** *A*, *blue diamonds* and *red squares* show the position of peaks obtained from one of the control sample datasets and one of the AAP-treated sample datasets, respectively. *B*, migration time shifts between corresponding peaks from the two datasets were fitted to the Reijenga's function as described in the main text. *C*, function was then used to rescale the timescale of the AAP treatment sample dataset.

decrease in GSH, which is a necessary cofactor for methionine adenosyltransferase (MAT) (28). Alternately, a possible inhibition of cystathionine β-synthase, the rate-limiting enzyme in the transsulfuration pathway might explain this finding. This can be suggested from the elevation of both methionine and serine levels without a concomitant increase in cystathionine levels at 2–6 h after AAP exposure (supplemental Fig. S3), although the detailed mechanism requires further examination.

Another major change in metabolite profiles of AAP-treated mice was the significant increase in abundance of an unidentified cationic metabolite of *m/z* 290.135 eluting at 16.5 min (Fig. 1) whose characterization is described in detail below.

Ophthalmate as Major Byproduct after AAP Treatment and Activation of Its Biosynthesis—Using tandem mass spectrometry with a CE-Q-TOFMS system, the precise MS/MS spectra of GSH (Fig. 5*A*) and the

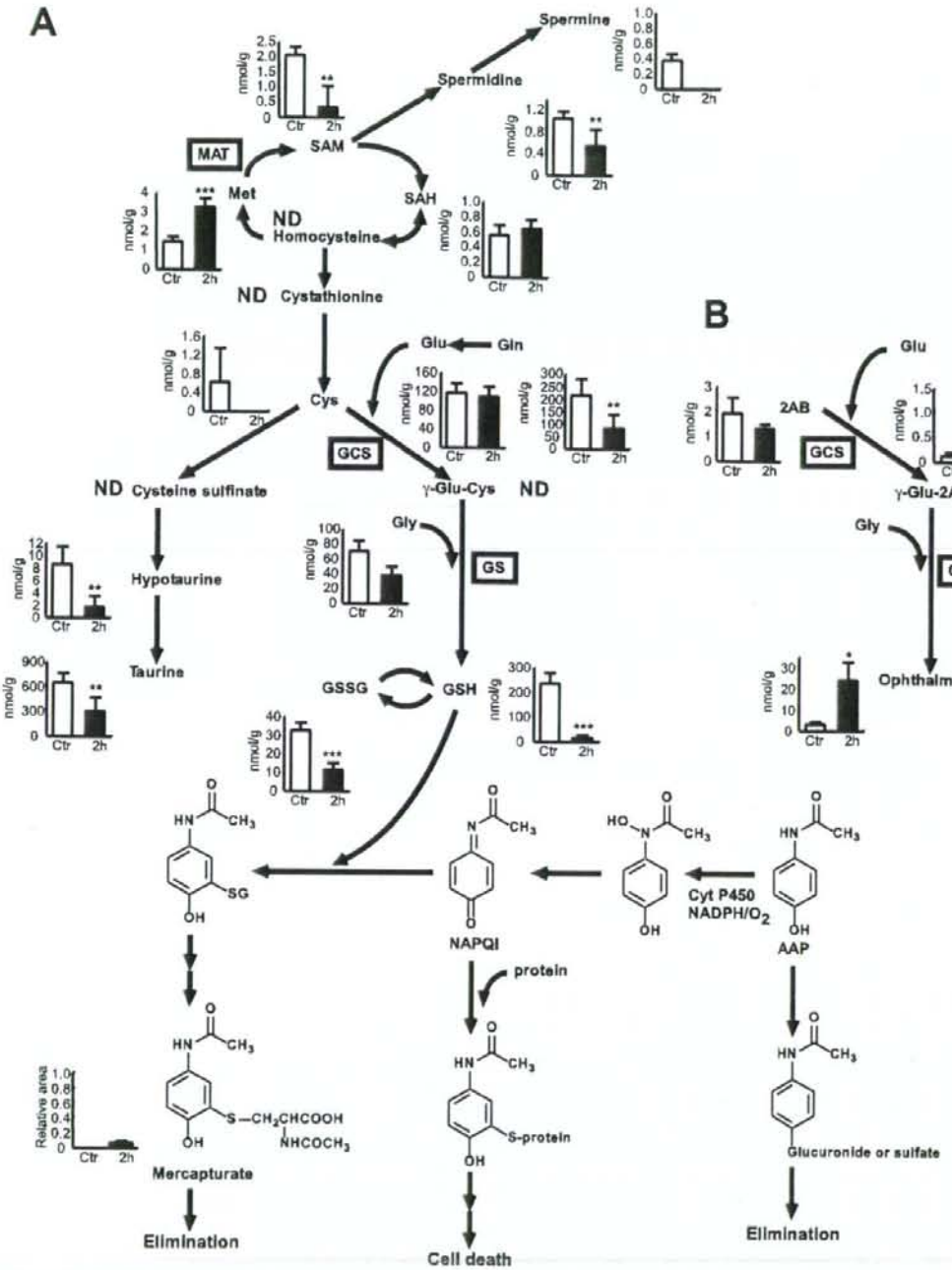

FIGURE 5. **Observed metabolite changes mapped onto the pathways involved in acetaminophen metabolism and its elimination.** *A*, changes in hepatic metabolite levels in the controls and mice injected 2 h earlier with AAP. The data were obtained by simultaneous analysis of charged metabolites using CE-TOFMS and correspond to the data shown in Fig. 1. *B*, changes in hepatic metabolite levels in the controls and mice injected 2 h earlier with AAP. The metabolites participate in the part of the pathway leading to ophthalmate biosynthesis. *Asterisks* indicate statistically significant differences. ***, $p < 0.001$; **, $p < 0.01$; *, $p < 0.05$.

unknown cation (*m/z* 290.135, 16.5 min) (Fig. 6*B*) obtained by CE-Q-TOFMS analysis of liver samples were carefully compared. The fragmentation patterns of GSH and the unknown cation were similar, and the mass difference between the four predominant peaks was just around 17.96 Da (indicated by *red dashed arrows* in Fig. 6). This suggested that the SH (32.980 Da) group in GSH might be replaced by a

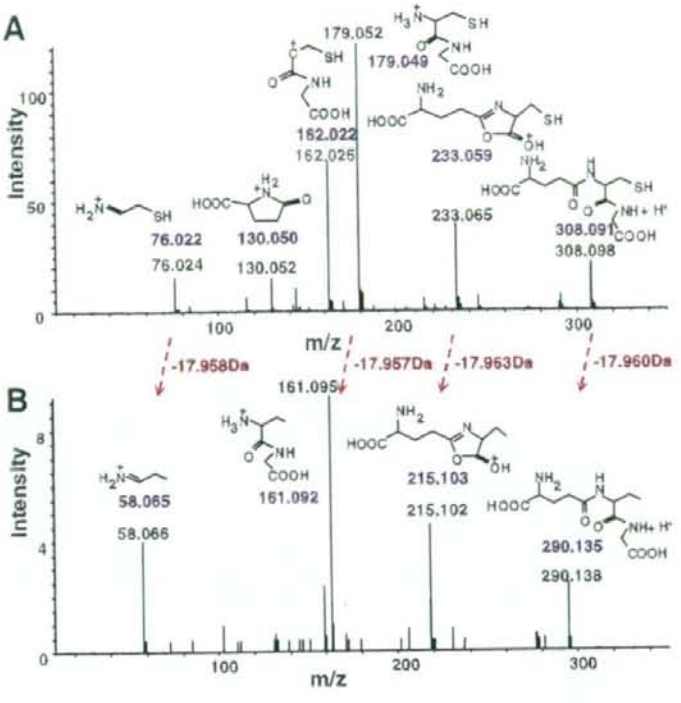

FIGURE 6. **MS/MS spectra of (*A*) GSH and (*B*) an unknown cation (*m/z* 290. 0135, 16.5 min) by CE-Q-TOFMS.** The chemical structures of the fragment ions and their *m/z* values (*blue*) (see supplemental Fig. S2), and the experimentally obtained *m/z* values for fragment ions (*black*) are displayed. The fragmentation patterns between GSH and the unknown cation are similar, and the mass difference between the four dominant peaks is close to 17.96 Da (*red dashed arrows*).

CH_3 (15.023 Da) group (32.980−15.023 Da = 17.957 Da) in the unknown compound. To confirm the position of the substitution within the GSH tripeptide (γ-Glu-Cys-Gly), we compared the MS/MS fragmentation pattern of both GSH and the unknown cation, the latter based on the structure of ophthalmate (see supplemental Fig. S2). We compared the *m/z* values of the predominant ions in the resulting compound (blue) with those from the experimentally determined MS/MS fragmentation ions (black) (Fig. 6, *A* and *B*) to assess their consistency. The results are consistent with the replacement of the SH group of the cysteine residue of GSH, with a CH_3 group to form 2-aminobutyrate (2AB) found in ophthalmate (γ-Glu-2AB-Gly). To confirm this, we obtained ophthalmate from commercial sources (Bachem, Bubendorf, Switzerland) and analyzed mouse liver samples spiked with the ophthalmate standard using CE-TOFMS and CE-Q-TOFMS. There was a perfect correspondence with respect to both migration time and MS/MS spectrum between ophthalmate and the unknown compound. This result thus leads us to conclude that the unidentified compound is indeed ophthalmate.

As ophthalmate is an analog of GSH, this finding raises the question of how the thiol group of cysteine in GSH is replaced by a methyl group in ophthalmate. As for GSH, ophthalmate can be synthesized *in vivo* from 2AB through consecutive reactions with γ-glutamylcysteine synthetase (GCS) and glutathione synthetase (GS) (Fig. 5*B*) (29). Further support for this biosynthetic route comes from previous reports that GCS catalyzes the ligation of glutamine and 2AB (30) and that GS can synthesize ophthalmate from γ-Glu-2AB (31). In agreement with this, the level of γ-Glu-2AB (*m/z* 233.113, 15.5 min), a substrate of GS, increased in the liver of AAP-treated mice (Fig. 5*B*). This finding suggests that GCS, the enzyme that is feedback-inhibited by GSH, and is a rate-limiting step in GSH synthesis (32, 33), was activated during GSH depletion and/or that GS may display lower affinity for γ-Glu-2AB compared with γ-Glu-Cys.

We further investigated ophthalmate metabolism by lowering the hepatic content of GSH by pretreating mice with BSO or DEM (Fig. 7*A*). BSO is known to result in significant GCS inhibition (34) and thus cause a reduction of downstream products. On the other hand, DEM leads to the oxidation of the thiol group in GSH (35) and the induction of lipid peroxidation and necrotic cell death (36). Liver and serum samples from control and BSO and DEM treated mice were analyzed in more detail by CE-TOFMS to identify specific changes in the levels of GSH/GSSG and ophthalmate and its precursors. As expected, the levels of GSH as well as γ-Glu-2AB and ophthalmate were very low both in the liver and serum of GCS-inhibited mice (Fig. 7, *A* and *B*). On the other hand, a marked increase in γ-Glu-2AB and ophthalmate levels was seen in DEM-treated mice. We can thus conclude that ophthalmate was synthesized using the same pathway as GSH. The results also suggest that GSH depletion by oxidative compounds such as AAP and DEM resulted in GCS activation, which in turn induced ophthalmate synthesis. However, unlike GSH, ophthalmate was not further metabolized and thus accumulated (Fig. 8).

Ophthalmate as an Oxystress Biomarker Indicating GSH Depletion—The above results in BSO- and DEM-treated mice indicate that a significant portion of these liver metabolites were effluxed to the circulation by the action of ATP-binding cassette (ABC) transporters such as multidrug resistance proteins (37) (Fig. 8). This close correspondence between hepatic and serum levels suggests the possibility that some of the detected compounds could act as biomarkers of GSH level alteration. In addition, the fact that both AAP and DEM result in GSH depletion and an increase in ophthalmate levels suggests that this response is not specific to AAP treatment but possibility reflects a more general cellular response to oxidative stress.

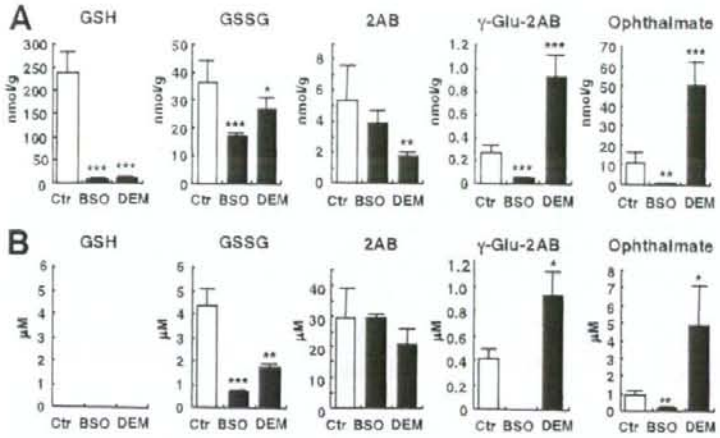

FIGURE 7. **Metabolite concentrations in (*A*) mouse liver ($n = 5$) and (*B*) serum ($n = 3$) 2 h after BSO or DEM treatment obtained by CE-TOFMS.** *Asterisks* indicate significant differences. ***, $p < 0.001$; **, $p < 0.01$; *, $p < 0.05$. No γ-Glu-Cys peak was detected.

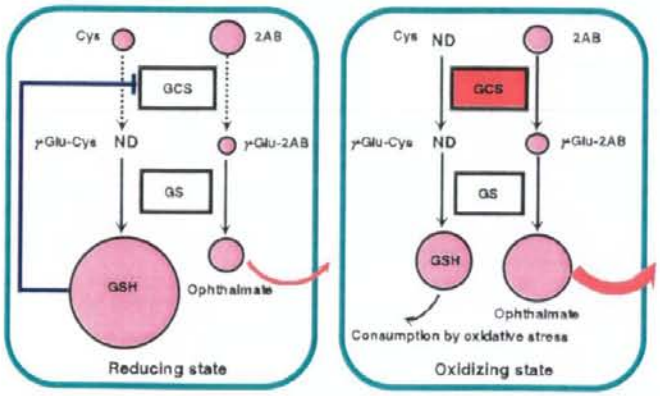

FIGURE 8. **Mechanism of ophthalmate biosynthesis in hepatocytes.** GCS is feedback-inhibited by GSH under reducing condition and little ophthalmate is thus synthesized. During oxidative stress, GSH is consumed, leading to GCS activation. This could result in biosynthesis of ophthalmate which is then effluxed across hepatocellular membrane through MRP transporters. The size of metabolite circles is proportional to their measured abundance in liver. *ND*, not detected.

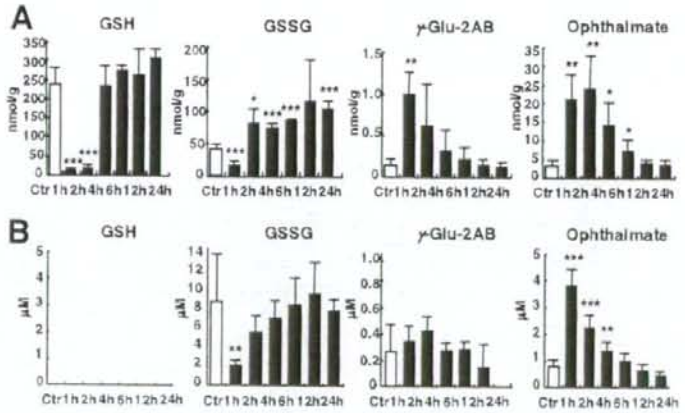

FIGURE 9. **Changes in metabolite levels in (*A*) mouse liver and (*B*) serum 1, 2, 4, 6, 12, and 24 h after AAP treatment ($n = 4$).** *Asterisks* indicate significant differences (***, $p < 0.001$; **, $p < 0.01$; *, $p < 0.05$). The hepatic GSH level at 1 h after AAP treatment was ~28-times lower than in the controls ($p < 1.6 \times 10^{-5}$). On the other hand, the ophthalmate level in mouse serum at 1 h after AAP treatment increased ~5-fold compared with the controls ($p = 0.0001$).

GSH, a ubiquitous and important antioxidant that protects mitochondria against endogenous oxygen radicals, is one of the most abundant intracellular antioxidants (38). GSH maintains enzymes and other cellular components in a reduced state (39) and its depletion leads to cell death. Therefore, biomarkers that can reveal disturbances in intracellular GSH levels can provide important information on the cellular reduction-oxidation (redox) state. We measured the levels of GSH, GSSG, γ-Glu-2AB, and ophthalmate, together with several metabolic intermediates of glutathione biosynthesis, in both liver and serum of mice at 1, 2, 4, 6, 12, and 24 h after AAP treatment. Most of the monitored metabolites that were detected in liver were also present in serum, but there was no significant difference in their concentration between control and AAP-treated mice (supplemental Fig. S3). On the other hand, significant increases in liver and serum ophthalmate levels were observed with

a concurrent hepatic GSH depletion in AAP treated mice (Fig. 9). Despite the high GSH levels in liver, GSH was not detected in serum suggesting that GSH is either not effluxed from liver, or that it is rapidly metabolized or oxidized in serum (40).

Serum ophthalmate increased ~5-fold ($p = 0.0001$) 1 h after AAP treatment, a point at which the liver GSH level dropped dramatically (Fig. 9). The change in hepatic ophthalmate was inversely proportional to the hepatic GSH level. These results thus identify serum ophthalmate level as a potential hepatic GSH biomarker that can reveal liver GSH abnormalities triggered by oxidative stress (Fig. 8).

Whereas hepatic γ-Glu-2AB increased 1 h after AAP treatment, serum γ-Glu-2AB did not increase significantly (Fig. 9), indicating that hepatic γ-Glu-2AB may not readily be exported to the circulation by ABC transporters or that, similarly to GSH, it is rapidly metabolized.

Overall, the time frame of changes in metabolites that we observed agrees very well with a previous report (9) showing a rapid (1–2 h) induction of multiple hepatic genes and their products following AAP administration in the mouse.

The physiological role of ophthalmate is not clearly established. In this work, it appears to be produced as a byproduct of the GS reaction when GSH, and consequently, cysteine levels are depleted. However, it has been previously suggested that ophthalmate may act as an anticoenzyme (41) that can inhibit enzymes that use GSH as a co-factor. GSH is normally exported in large proportion by the liver into bile and circulation to be used in peripheral tissues (42). Interestingly, ophthalmate was shown to competitively inhibit and trans-stimulate GSH uptake in liver canalicular membranes (43). This may help minimize GSH efflux from liver cells during oxidative stress.

GSH is conjugated to many types of exogenous metabolites such as AAP to increase their solubility and facilitate their excretion. GSH also enhances multidrug resistance protein 1 (MRP1)-mediated transport of the glucoronide conjugate of the tobacco carcinogen 4-(methylnitrosamino)-1-(3-pyridyl)-1-butanol (NNAL) and ophthalmate can substitute for this activity (44, 45). Ophthalmate can thus act as a GSH analog for functions that do not require the presence of the thiol group such as activation of transport of exogenous metabolite glucoronides by MRP1. It is thus tempting to speculate that ophthalmate might similarly stimulate the transport of AAP-glucoronide by MRP1 and thus facilitate its elimination. This would provide functional meaning for its synthesis during oxidative stress rather than simply being a consequence or byproduct of cysteine/GSH depletion and the associated activation of GCS.

Because of differences in the analytical methods, our results seem complementary to previous work by Coen *et al.* (46, 47) who profiled changes in liver metabolites following AAP treatment using NMR. Whereas these authors examined mostly neutral and lipid metabolites, our work using CE-MS and focusing on polar metabolites demonstrates the consequences of GSH depletion and the attempts of the liver to increase its biosynthesis. On the other hand, Coen *et al.* (46, 47) reported an activation of glycolysis while lipid metabolism was decreased and this may reflect the energy and precursor requirements for GSH and related metabolites biosynthesis as well as mitochondrial damage, respectively. Both studies concur regarding increases in the level of several amino acids, which can be measured by both NMR and CE-TOFMS levels.

We presented a sensitive and high resolution metabolome differential display approach, based on a CE-TOFMS system and data analysis software, that facilitates the global quantification and identification of charged metabolites as well as the visualization of specific changes in complex biological matrices. This approach can be applied to the discovery of biomarkers as we demonstrated by the identification of serum ophthalmate as a biomarker for hepatic GSH depletion following oxidative stress. Ophthalmate measurement can potentially provide valuable information about the hepatic cellular redox state, thereby facilitating the earlier prediction of oxidative damage. This biomarker may thus help to evaluate therapeutic risks, efficacy, and drug actions during the drug development process and potentially facilitate the early detection of several diseases (such as Alzheimers, Parkinsons, and liver disease, AIDS, cancer, cardiac infarction, and diabetes) (48), where oxidative stress is known to play an important role.

Acknowledgments—We thank Kenjiro Kami, Natsumi Saito, Masahiro Sugimoto, Noriyuki Sugiyama, and Mineo Morohashi for technical advice and support.

REFERENCES

1. Vermeulen, N. P., Bessems, J. G., and Van de Straat, R. (1992) *Drug Metab. Rev.* **24,** 367–407
2. Dahlin, D. C., Miwa, G. T., Lu, A. Y., and Nelson, S. D. (1984) *Proc. Natl. Acad. Sci. U. S. A.* **81,** 1327–1331
3. Vendemiale, G., Grattagliano, I., Altomare, E., Turturro, N., and Guerrieri, F. (1996) *Biochem. Pharmacol.* **52,** 1147–1154
4. Mitchell, J. R., Jollow, D. J., Potter, W. Z., Davis, D. C., Gillette, J. R., and Brodie, B. B. (1973) *J. Pharmacol. Exp. Ther.* **187,** 185–194
5. Gibson, J. D., Pumford, N. R., Samokyszyn, V. M., and Hinson, J. A. (1996) *Chem. Res. Toxicol.* **9,** 580–585
6. Wallace, J. L. (2004) *Br. J. Pharmacol.* **143,** 1–2
7. Hinson, J. A., Reid, A. B., McCullough, S. S., and James, L. P. (2004) *Drug Metab. Rev.* **36,** 805–822
8. Reilly, T. P., Bourdi, M., Brady, J. N., Pise-Masison, C. A., Radonovich, M. F., George, J. W., and Pohl, L. R. (2001) *Biochem. Biophys. Res. Commun.* **282,** 321–328
9. Ruepp, S. U., Tonge, R. P., Shaw, J., Wallis, N., and Pognan, F. (2002) *Toxicol. Sci.* **65,** 135–150
10. Raamsdonk, L. M., Teusink, B., Broadhurst, D., Zhang, N., Hayes, A., Walsh, M. C., Berden, J. A., Brindle, K. M., Kell, D. B., Rowland, J. J., Westerhoff, H. V., van Dam, K., and Oliver, S. G. (2001) *Nat. Biotechnol.* **19,** 45–50
11. Spinnler, H. E., Ginies, C., Khan, J. A., and Vulfson, E. N. (1996) *Proc. Natl. Acad. Sci. U. S. A.* **93,** 3373–3376
12. Ideker, T., Thorsson, V., Ranish, J. A., Christmas, R., Buhler, J., Eng, J. K., Bumgarner, R., Goodlett, D. R., Aebersold, R., and Hood, L. (2001) *Science* **292,** 929–934
13. Fraenkel, D. G. (1992) *Annu. Rev. Genet.* **26,** 159–177
14. Fernie, A. R., Trethewey, R. N., Krotzky, A. J., and Willmitzer, L. (2004) *Nat. Rev. Mol. Cell. Biol.* **5,** 763–769
15. Fiehn, O., Kopka, J., Dormann, P., Altmann, T., Trethewey, R. N., and Willmitzer, L. (2000) *Nat. Biotechnol.* **18,** 1157–1161
16. Plumb, R., Granger, J., Stumpf, C., Wilson, I. D., Evans, J. A., and Lenz, E. M. (2003) *Analyst* **128,** 819–823
17. Reo, N. V. (2002) *Drug Chem. Toxicol.* **25,** 375–382
18. Aharoni, A., Ric de Vos, C. H., Verhoeven, H. A., Maliepaard, C. A., Kruppa, G., Bino, R., and Goodenowe, D. B. (2002) *Omics* **6,** 217–234
19. Soga, T., Ohashi, Y., Ueno, Y., Naraoka, H., Tomita, M., and Nishioka, T. (2003) *J. Proteome. Res.* **2,** 488–494
20. Shiomi, M., Wakabayashi, Y., Sano, T., Shinoda, Y., Nimura, Y., Ishimura, Y., and Suematsu, M. (1998) *Hepatology* **27,** 108–115
21. Soga, T., and Heiger, D. N. (2000) *Anal. Chem.* **72,** 1236–1241
22. Katayama, H., Ishihama, Y., and Asakawa, N. (1998) *Anal. Chem.* **70,** 5272–5277
23. Soga, T., Ueno, Y., Naraoka, H., Ohashi, Y., Tomita, M., and Nishioka, T. (2002) *Anal. Chem.* **74,** 2233–2239
24. Douglas, D. H., and Peucker, T. K. (1973) *Can. Cartographer* **10,** 112–122
25. Palmer, M. E., Clench, M. R., Tetler, L. W., and Little, D. R. (1999) *Raid Commun. Mass Spectrom.* **13,** 256–263
26. Reijenga, J. C., Martens, J. H. P. A., Giuliani, A., and Chiari, M. (2002) *J. Chromatogr. B* **770,** 45–51
27. Goto, S., Okuno, Y., Hattori, M., Nishioka, T., and Kanehisa, M. (2002) *Nucleic Acids Res.* **30,** 402–404
28. Corrales, F. J., Ruiz, F., and Mato, J. M. (1999) *J. Hepatol.* **31,** 887–894
29. Orlowski, M., and Wilk, S. (1978) *Biochem. J.* **170,** 415–419
30. Huang, C. S., Moore, W. R., and Meister, A. (1988) *Proc. Natl. Acad. Sci. U. S. A.* **85,** 2464–2468
31. Oppenheimer, L., Wellner, V. P., Griffith, O. W., and Meister, A. (1979) *J. Biol. Chem.* **254,** 5184–5190
32. Richman, P. G., and Meister, A. (1975) *J. Biol. Chem.* **250,** 1422–1426

33. Cuozzo, J. W., and Kaiser, C. A. (1999) *Nat. Cell Biol.* **1,** 130–135
34. Griffith, O. W., and Meister, A. (1979) *J. Biol. Chem.* **254,** 7558–7560
35. Zalups, R. K., and Lash, L. H. (1997) *Drug Metab. Dispos.* **25,** 516–523
36. Tirmenstein, M. A., Nicholls-Grzemski, F. A., Zhang, J. G., and Fariss, M. W. (2000) *Chem. Biol. Interact.* **127,** 201–217
37. Keppler, D., Leier, I., and Jedlitschky, G. (1997) *Biol. Chem.* **378,** 787–791
38. Yang, C. S., Chen, W. Y., Tsai, P. J., Cheng, F. C., and Kuo, J. S. (1997) *Biochem. Pharmacol.* **53,** 357–361
39. Meister, A. (1995) *Methods Enzymol.* **251,** 3–7
40. Joshi, U. M., Rao, K. S., and Mehendale, H. M. (1987) *Int. J. Biochem.* **19,** 1029–1035
41. Waley, S. G. (1953) *Bioclim. Biophys. Acta* **10,** 27–34
42. Meister, A., and Anderson, M. E. (1983) *Annu. Rev. Biochem.* **52,** 711–760
43. Ballatori, N., and Dutczak, W. J. (1994) *J. Biol. Chem.* **269,** 19731–19737
44. Leslie, E. M., Ito, K., Upadhyaya, P., Hecht, S. S., Deeley, R. G., and Cole, S. P. (2001) *J. Biol. Chem.* **276,** 27846–27854
45. Leslie, E. M., Bowers, R. J., Deeley, R. G., and Cole, S. P. (2003) *J. Pharmacol. Exp. Ther.* **304,** 643–653
46. Coen, M., Lenz, E. M., Nicholson, J. K., Wilson, I. D., Pognan, F., and Lindon, J. C. (2003) *Chem. Res. Toxicol.* **16,** 295–303
47. Coen, M., Ruepp, S. U., Lindon, J. C., Nicholson, J. K., Pognan, F., Lenz, E. M., and Wilson, I. D. (2004) *J. Pharm. Biomed. Anal.* **35,** 93–105
48. Wu, G., Fang, Y. Z., Yang, S., Lupton, J. R., and Turner, N. D. (2004) *J. Nutr.* **134,** 489–492

ANTIOXIDANTS & REDOX SIGNALING
Volume 8, Numbers 9 & 10, 2006

Forum Original Research Communication

Erythrocytes with T-State–Stabilized Hemoglobin as a Therapeutic Tool for Postischemic Liver Dysfunction

KAZUHIRO SUGANUMA,*[,1] KOSUKE TSUKADA,*[,1] MISATO KASHIBA,[1]
ANTONIO TSUNESHIGE,[3] TOSHIHARU FURUKAWA,[2] TETSURO KUBOTA,[2]
NOBUHITO GODA,[1] MASAKI KITAJIMA,[2] TAKASHI YONETANI,[3] and MAKOTO SUEMATSU[1]

ABSTRACT

This study aimed to examine if T-state stabilization of hemoglobin in erythrocytes could protect against postischemic organ injury. Human erythrocytes containing three different states of Hb allostery were prepared: control Hb (hRBC), CO–Hb that is stabilized under R-state with the 6-coodinated prosthetic heme (CO-hRBC), and α-NO-deoxyHb stabilized under T-state (α-NO-hRBC). To prepare α-NO-RBC, deoxygenated RBC was treated with FK409, a thiol-free NO donor, at its half molar concentration to that of Hb; this procedure resulted in the 5-coordinated NO binding on the α-subunit heme, as judged by electron spin resonance spectrometry. Rats were subject to 20 min systemic hemorrhage to maintain mean arterial pressure at 40 mm Hg, and reperfused with one of hRBCs. This protocol for ischemia, followed by 60 min reperfusion with physiological saline, caused modest metabolic acidosis and cholestasis. Administration of hRBC or CO-hRBC significantly attenuated cholestasis and improved acidosis. Rats treated with α-NO-hRBC exhibited greater recovery of metabolic acidosis and bile excretion than those treated with hRBC or CO-hRBC, displaying the best outcome of local oxygen utilization in hepatic lobules. Half-life time of α-NO-RBC administered *in vivo* was approximately 60 min. These results suggest that T-state Hb stabilization by NO serves as a stratagem to treat postischemic organ dysfunction. *Antioxid. Redox Signal.* 8, 1847–1855.

INTRODUCTION

THERE ARE SEVERAL LINES of evidence that allostery of hemoglobin (Hb) does not only determine the oxygen-carrying capacity of red blood cells (RBC) but also dictates an oxygen-sensing ability to regulate microvascular function. RBC can sense a reduction of PO_2 and an increase in PCO_2 by utilizing Hb: such alterations in local gas tension have been shown to cause conformational stabilization of T-state Hb, which is characterized by a 5-coordinated structure of the prosthetic heme, and thereby facilitate the release of molecular oxygen from Hb in the peripheral tissue, known as Bohr's effect (31). On the other hand, an elevation of PO_2 or partial binding of carbon monoxide (CO) stabilizes R-state Hb, which is characterized by the 6-coordinated heme structure. The latter mechanism renders Hb ineffective in its delivery of O_2 to peripheral tissues, which is the primary cause of CO poisoning. The Hb allostery of this kind has been reported to regulate microvascular function through multiple mechanisms. First, alterations in the Hb allostery play a key role in regulation of the delivery of NO released from the cells (19, 24). Under the low oxygen tension where T-state Hb is stabilized, the release of RBC-derived NO is brought to the microvascular endothelium and helps vasorelaxation to guarantee an ample blood supply in hypoxic regions (10). RBC also have the ability to release ATP in response to hypoxia (3). As

[1]Department of Biochemistry and Integrative Medical Biology and [2]Department of Surgery, School of Medicine, Keio University, Tokyo, Japan; [3]Department of Biochemistry and Biophysics, School of Medicine, University of Pennsylvania, Philadelphia, Pennsylvania.
*KS and KT equally contributed to this work as the first author.

previously shown, extracellularly released ATP activates purinergic receptors on endothelial cells to trigger intracellular calcium ion and NO generation (6, 7). Such hypoxic responses of RBC appear to result from allosteric changes in Hb, so far as judged from the observation that CO, the R-state stabilizer, significantly diminished hypoxia-induced ATP release from the cells (6, 9).

Although neither mechanisms *in vivo* by which NO is degraded in and around RBC nor those resulting in hypoxia-triggered conductance of NO or ATP across RBC membrane have been well described yet (5, 14), these results tempted us to investigate if stationary stabilization of the T-state Hb allostery could serve as a therapeutic tool for improving hypoxic organ damages, since RBC with T-state stabilized Hb might have a greater ability to release oxygen and to trigger vasorelaxation for maintenance of ample blood supply than normal RBC. Recent studies revealed that T-state Hb can be stabilized without destroying RBC by treating the cells with membrane-diffusable NO under deoxygenated conditions (30, 31). In these studies, α-nitrosyl Hb, α-$(Fe\text{-}NO)_{2\beta}(Fe)_2$ has been synthetically prepared. Despite the halved O_2-carrying capacity, α-nitrosyl Hb could represent a versatile low affinity O_2 carrier with improved features that might deliver O_2 to tissues effectively even after NO is sequestered at the heme site of Hb. However, solid evidence for effectiveness of RBC with α-nitrosyl Hb to treat hypoxic organ dysfunction *in vivo* and its pathophysiologic link to local O_2 metabolism have not fully been investigated *in vivo*. This study was designed to examine the protective effects of RBC with α-nitrosyl Hb on microvascular function, O_2 delivery, and organ function in the postischemic rat liver where the O_2 delivery is limited even under physiologic conditions.

MATERIALS AND METHODS

Preparation and characterization of α-nitrosyl Hb in human erythrocytes

Human erythrocytes (RBC) were isolated from heparinized peripheral blood samples collected from healthy male volunteers who gave informed consents. The blood samples were centrifuged at 2,000 *g* for 10 min and washed twice with modified SAGM buffer solution. Hb in the RBCs was fully deoxygenated by gentle purge for 30 min with highly purified argon gas under acidic pH conditions, as described previously (30). A portion of the RBC-suspended solution was sampled and hemolyzed to determine Hb concentrations by measuring visible absorption spectra at 540 nm. Under maintenance of the temperature at 4°C, an NO donor, FK409 (a generous gift from Fujisama Pharmaceutical Inc., Osaka) was added to the RBC suspension at a half concentration of Hb in the suspension (30). This NO-donating reagent has the ability to release equimolar amounts of NO in the aqueous solution. Distinct from other NO donors such as *S*-nitroso glutathione, FK409 does not contain a sulfhydryl group in its chemical structure; such an advantage allowed us to avoid a possible contamination of exogenous *S*-nitrosothiols in experiments.

Structural characterization of the prosthetic heme of Hb by binding of NO was carried out by electron spin resonance (EPR) spectrometry, according to the previous method (31). To this end, a portion of the NO-treated RBC were frozen at 77°K with liquid nitrogen to serve as a sample to detect triplet peaks, indicating a 5-coordinated structure of the heme of two α-subunits of Hb in the whole cell suspension (30). The 5-coordinated structure of the prosthetic heme of Hb was demonstrated by an EPR spectrometer (JEOL, Tokyo, Japan), as described elsewhere with minor modifications (30, 31). Briefly, the power and frequency of microwave were 1.0 mW and 9.1 GHz, respectively. Time duration and a range for scanning the EPR signal were 0.5 min and 326 ± 25 mT, respectively. Unless mentioned, the NO-treated RBC sample was designated as α-NO-hRBC, unless mentioned otherwise. Separately, the control and CO-saturated RBC samples were prepared at 4°C and designated as hRBC and CO-hRBC, respectively. The Hb concentration of these RBC samples was prepared at 10 g/dl by adding the physiological saline and stored at 4°C until the animal experiments. The RBC samples were incubated at 37°C at 30 min prior to the start of the experiments *in vivo*.

In vivo *experimental protocols for hemorrhage-induced liver dysfunction*

The experimental protocols herein described were approved by our institutional guidelines provided by the Animal Care Committee of Keio University School of Medicine. Male Wistar rats weighing 240–280 g (CLEA Japan, Tokyo) were allowed free access to laboratory chow and tap water, and were fasted for 24 h prior to experiments. As described elsewhere (21, 23), rats were anesthetized with an intramuscular injection of pentobarbital sodium at 50 mg/kg, and their common bile duct and carotid and femoral arteries were cannulated to collect bile and blood samples, respectively. Bile output was monitored *in vivo* according to our previous method (4, 13). The femoral arterial cannulation was used to monitor systemic blood pressure and heart rate (HR). The carotid cannulation was to withdraw blood from circulation and to collect blood samples for blood-gas analyses. The arterial PO_2, pH, and concentrations of HCO_3^- and Hb were determined in the arterial blood samples, using the gas analyzer as described elsewhere (8, 18, 25). Based on determination of these parameters, base excess (BE) was also calculated as an index of metabolic acidosis. When necessary, pulse-Doppler flowmetry was conducted to measure visceral blood flow in the abdominal aorta.

Rats were exposed to acute hemorrhage by letting them bleed from a carotid arterial catheter, according to the protocol described previously (29). The mean arterial pressure (MAP) was maintained at 40 mm Hg for 20 min. The shed blood was collected in heparinized syringes and the volume was measured. The blood was kept at 37°C to be reinfused as autologous blood samples, when necessary. After completing the 20-min hypovolemic ischemia, one of hRBC was infused at 1 ml/min at a total volume equivalent to that of shed blood.

In vivo *monitoring of hepatic microcirculation and local oxygen tension*

In separate sets of experiments, rats used to observe hepatic microcirculation were prepared with tracheotomy to

establish the airway for inhalational anesthesia with sevoflurane, as described in our previous method (16). The anesthetized rats underwent midline and pericostal incisions to expose the left lobe of the liver. The current choice of anesthesia allowed us to guarantee stability of systemic blood pressure during 4 h observation of the left lobular portion of the liver surface. The exteriorized portion of the liver was set on the cover glass mounted in the plastic stage and observed through an inverted-type fluorescence microscope equipped with an high-speed video analyzing device combined with a photomultiplier to measure partial oxygen tension (PO_2) in microvessels by analyzing phosphorescence decay (20). When necessary, erythrocytes suspended in physiological saline were prepared by whole blood samples taken from donor rats and labeled with fluorescein isothiocyanate (FITC), according to our previous method (8, 29). Each rat received 100 μl of FITC-labeled RBC suspension through an intravenous injection.

For microvascular PO_2 measurements, Pd-meso-tetra-(4-carboxyphenyl)-porphyrin (Pd-TCPP, Porphyrin Products, Eugene, OR) was used as a phosphorescence probe indicating O_2-dependent quenching of the light emission (20, 29). The reagent was dissolved at 20 mg/ml in physiological saline containing bovine serum albumin and buffered at pH 7.4 with phosphate buffer. Rats received a slow bolus of Pd-TCPP at 30 mg/kg through an intravenous injection. Pd-TCPP circulating in hepatic central venules was excited by using the second harmonic of a Q-switched Nd/YAG pulse laser at 532 nm with 6-nsec pulse width, according to the previous method (29). Phosphorescence passing through a long-pass filter (>620 nm) was detected with a photomultiplier tube (R1894, Hamamatsu Photonics, Hamamatsu City, Shizuoka). The voltage signal was fed into a computer via an analog-to-digital converter (NR-2000, Keyence, Tokyo) with a sampling frequency of 200 kHz and sampling number of 500 points. PO_2 values were calculated based on the Stern–Volmer equation, as described elsewhere (20, 29).

To measure the RBC velocity and PO_2 at 1 Hz, we used a mechanical shutter to control the output of a mercury lamp and used the signal from a limit switch to trigger the Nd/YAG laser when the shutter was closed. The irradiation times of the laser and mercury lamp were 6 nsec and 300 msec, respectively. PO_2 values in central venules were measured as a function of time before and after exposure to the 20-min hypovolemic ischemia. Alterations in sinusoidal diameter, functional sinusoidal density, and RBC velocity and local intravascular PO_2 in central venules were compared between postischemic livers treated with hRBC and those treated with α-NO-hRBC. These measurements were performed before and 5, 10, 15, 30, and 60 min after the start of reperfusion.

Determination of half lifetime of exogenously administered α-NOHb in circulation

To determine the half-life time of α-NO-hRBC, 2 ml of the peripheral blood samples were collected from the carotid artery of rats, which were exposed to the 20-min hypovolemic ischemia, followed by desired duration of time for reperfusion of one of the hRBC samples. The collected blood samples were immediately frozen by liquid nitrogen at 77°K to serve as samples for EPR spectrometry. As described later in Results, α-nitrosyl heme was undetectable in peripheral blood samples collected from the control and the postischemic rats reperfused with autologous blood samples, indicating that the amount of endogenous α-NOHb-containing rat erythrocytes is little in circulation, if any. In these experiments, the putative concentrations of circulating α-NOHb were calculated as a function of time for reperfusion. To this end, the circulating concentration of the Hb derived from hRBC administered exogenously was calculated, assuming that the total blood volume of the rat is 7% of the body weight. The α-NO-Hb concentrations were thus estimated by multiplying the concentrations of hRBC-derived Hb in the circulation and the percentage magnitude of the EPR triplet signal versus the initial magnitude measured at 5 min after reperfusion. This value of the nitrosyl Hb in circulation was designated as estimated nitrosyl-Hb concentrations, assuming that NO initially bound to αheme of hRBC Hb does not move to rat RBC-derived Hb in circulation.

Statistical analyses

Differences in mean values among groups were analyzed by ANOVA with Fisher's multiple comparison test. P values <0.05 were considered statistically significant.

RESULTS

Characterization of α-NO-hRBC in vitro *and* in vivo

Figure 1 illustrates the characterization of α-NO-hRBC *in vitro*. In these experiments, hRBC was fully deoxygenated with pretreatment with O_2-free Ar gas prior to the addition of the NO donor FK409. As seen in a representative EPR spec-

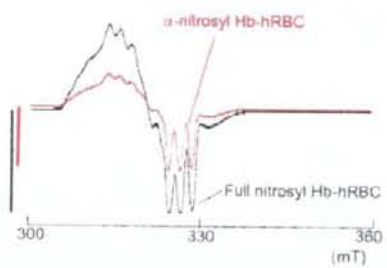

FIG. 1. Characterization of α-NO-human erythrocytes (α-NO-hRBC) prepared *in vitro* by electron paramagnetic resonance (EPR) spectrometry. A representative EPR signal of α-NO-hRBC with typical triplet signals indicating the 5-coordinated heme-NO complex. When FK409, a thiol-free NO donor, was added to the hRBC suspension at a half concentration versus Hb-associated heme concentration, the height of the triplet signal became about 50% versus that for hRBC treated with saturated concentrations of the NO donor (tetranitrosyl Hb). Considering an extremely greater affinity of NO to the α-subunit heme than to β-subunit one, these results suggest that exogenously applied NO is bound to the heme of α-subunits, forming 5-coordinated structure. *Black* and *red bars*: intensities of triplet signals in full nitrosyl and α-nitrosyl Hbs, respectively.

trum in the upper panel, the heights of the triplet signal for α-NO-hRBC prepared by the current protocol and that for hRBC fully saturated with NO were 0.78 and 1.53, respectively. These results indicate that the ratio of α-NOHb versus fully nitrosyl Hb was 0.51, suggesting that halves of the prosthetic heme are occupied with NO in αNO-hRBC.

We next examined the half lifetime of α-$(Fe\text{-}NO)_{2\beta}(Fe)_2$Hb of exogenously administered hRBC in the postischemic rats. As seen in the upper panel of Fig. 2, immediately after the α-NO-hRBC administration (T5) the triplet signal was detectable in systemic circulation. The height of the signal became weakened as a function of time after reperfusion. Such a decay of the triplet signal as a function of time for reperfusion was analyzed in three separate experiments (lower panel). In these experiments, the rate of blood replacement with α-NO-Hb hRBC was approximately 32%, and the average Hb concentration was 16.3 g/dl; apparent concentration of α-NO-Hb at 5 min after the start of reperfusion was approximately 5.0 g/dl. The concentrations of the circulating nitrosyl Hb were decreased as a function of time for reperfusion, indicating that the half life time of α-NOHb is approximately 60 min *in vivo*.

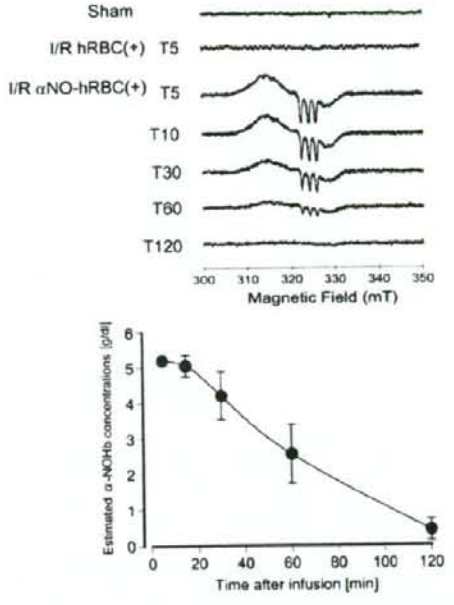

FIG. 2. Determination of exogenously administered α-NO-hRBC by EPR spectrometry in systemic blood samples in rats exposed to ischemia–reperfusion. *Upper panel*: Representative time history of the decay of α-NOHb-associated triplet signals in the blood samples. Sham and I/R hRBC(+); EPR signals of peripheral blood samples collected from sham-operated rats and from rats exposed to ischemia followed by 5-min reperfusion with hRBC, respectively. I/R α-NO-hRBC(+); temporal alterations in the EPR signals from rats reperfused with α-NO-hRBC. Measurements were carried out at 5, 10, 30, 60, and 120 min after the onset of reperfusion. *Lower panel:* Decay of the magnitude of the triplet signal as a function of time for reperfusion. Data denote the relative intensities versus the maximum value measured at 5 min and indicate mean ± SE of three separate experiments. Note that half-life time of α-NOHb is approximately 60 min in systemic circulation.

α-NO-hRBC improves recovery of visceral blood flow and bile output

We examined whether different modification of Hb allostery (α-NO-hRBC, hRBC, and CO-hRBC) could cause any differences in blood supply at the level of macrocirculation *in vivo*. As seen in Fig. 3, temporal alterations in MAP showed no significant differences and displayed a comparable recovery to the baseline during resuscitation among the three groups. HR values in the α-NO-hRBC-treated group were also comparable to those in the hRBC-treated group, while those treated with CO-hRBC group exhibited an incomplete recovery with no statistical significance versus other two groups (middle panel). During the 20-min period of hypovolemic hypoxia, visceral blood flow decreased by 50%

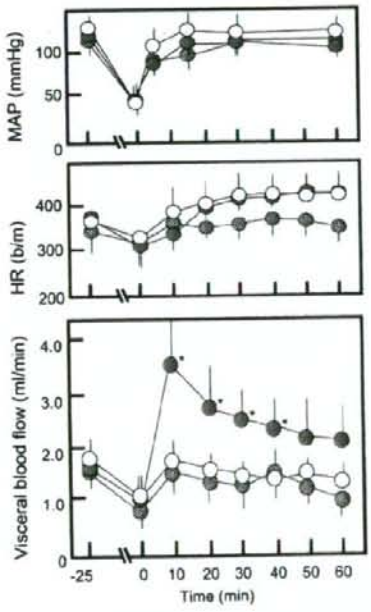

FIG. 3. Temporal alterations in mean arterial pressure (MAP), heart rate (HR), and visceral blood flow of rats exposed to the 20-min hypovolemic ischemia, followed by reperfusion with hRBC (*open circles*), CO-hRBC (*striped circles*), and α-NO-hRBC (*shaded circles*). Data indicate mean ± SE of five to seven separate experiments for each group. *$p < 0.05$ as compared with sham-operated controls. Note that α-NO-hRBC significantly increases splanchnic blood flow without altering MAP, suggesting a decrease in systemic vascular resistance.

of the preischemic control period in all groups. Upon reperfusion, rats administered with hRBC or with CO-hRBC displayed a recovery towards the control levels, while those treated with α-NO-hRBC indicated approximately twofold elevation of the flow at the early phase of reperfusion, which was followed by a gradual decay in the later period. Such a feature of the α-NO-hRBC-treated rats distinct from those treated with hRBC or with CO-hRBC was also evident in the recovery of bile output from the postischemic liver (Fig. 4). To be noted, no significant difference in the recovery of visceral blood supply and bile output during reperfusion was seen between CO-hRBC- and hRBC-treated groups, although both groups exhibited a significant recovery of bile output as compared with the group treated with physiological saline.

Potent improving effects of α-NO-hRBC on metabolic acidosis

In the current experimental model, the replacement of the shed blood with reperfusion with physiological saline induced significant decreases in arterial blood pH and base excess, when the data were compared among the groups at 60 min after the start of reperfusion (solid bars in Fig. 5). These results indicated that the protocol for hypovolemia followed by the 60-min reperfusion of the saline caused metabolic acidosis modestly but evidently. On the other hand, reperfusion with hRBC or with CO-hRBC significantly improved alterations in these parameters; the recovery of MAP is almost comparable to the sham-operated baseline level, while that of pH and base excess was partial so far. The recovery of these parameters for metabolic acidosis became more evident in the group treated with α-NO-hRBC than in the groups treated with hRBC or CO-hRBC, while the improvement of MAP was comparable among these three groups (Fig. 5). As shown in Fig. 3, the group treated with α-NO-hRBC displayed a greater increase in visceral blood flow than that treated with hRBC transiently at the early phase of reperfusion. However, at 60 min after the onset of reperfusion, the two groups did not show any notable differences in MAP and the visceral blood flow, while the α-NO-hRBC-treated group indicated the greatest recovery of bile output. This observation tempted us to examine if the time history of the recovery of local microvascular hemodynamics and oxygen utilization was different during the reperfusion period between the α-NO-hRBC- and hRBC-treated groups.

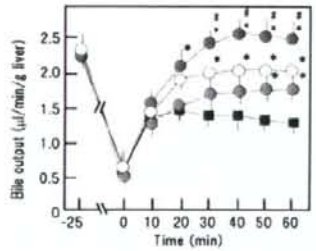

FIG. 4. Temporal alterations in bile output of rats exposed to the 20-min hypovolemic ischemia, followed by reperfusion with hRBC (*open circles*), CO-hRBC (*striped circles*), and α NO-hRBC (*shaded circles*). *Closed squares*; rats exposed to the ischemia followed by reperfusion with physiological saline (PS). Data indicate mean ± SE of six to eight separate experiments for each group. $*p < 0.05$ as compared with the PS-treated group. $\#p < 0.05$ as compared with the values for the hRBC-treated group.

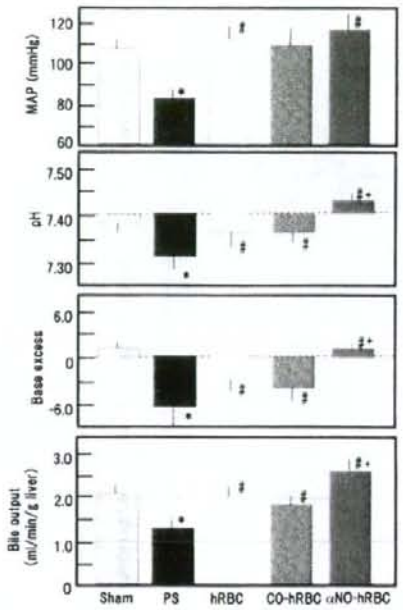

FIG. 5. Effects of postischemic administration of hRBC, CO-hRBC, and α-NO-hRBC on alterations in mean arterial pressure (MAP), pH, and base excess in arterial blood, and bile output of rats exposed to the 20-min hypovolemic ischemia, followed by 60-min reperfusion. The administration of one of these hRBCs or physiological saline (PS) was completed at 5 min after the start of reperfusion. Sham: data collected from sham-operated controls. Data indicate mean ± SE of 10–12 separate experiments for each group. $*p < 0.05$ as compared with sham-operated controls. $\#p < 0.05$ as compared with the values for the PS-treated group. $'p < 0.05$ as compared with the values for the hRBC-treated group. Note that rats treated with α-NO-hRBC displays the best outcomes of recovery from metabolic acidosis and cholestasis among the groups examined.

Distinct effects of α-NO-hRBC on the recovery of hepatic microvascular PO_2

Figure 6 illustrates the effects of the α-NO-hRBC administration on alterations in sinusoidal diameter, functional sinusoidal density, RBC velocity, and PO_2 in the central venules of postischemic liver lobules and a comparison of effects of the hRBC administration. At sinusoidal levels (a large circle in Panel A), temporal alterations in the diameter of microvessels (Panel B), and functional sinusoidal density

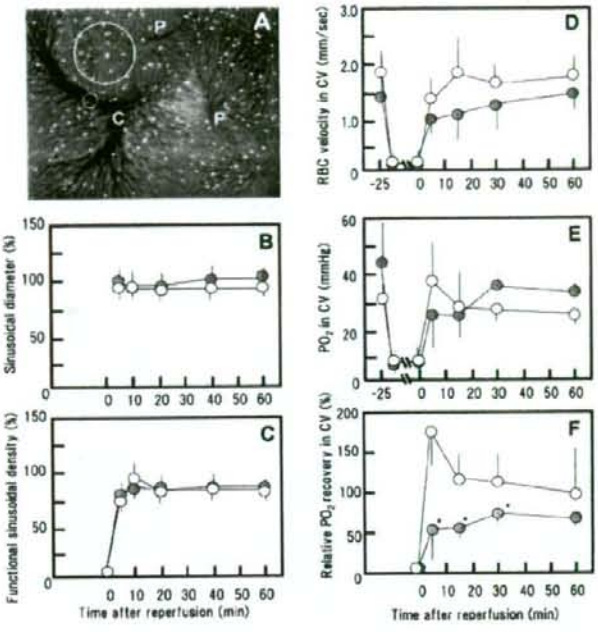

FIG. 6. Effects of the α-NO-hRBC administration on alterations in sinusoidal diameter, functional sinusoidal density, RBC velocity, and PO_2 in central venules of postischemic liver lobules. (**A**) A representative picture showing traffics of FITC-labeled RBC in the rat hepatic microcirculation. P and C; portal and central venules. *Large* and *small circles* indicate regions for determination of functional sinusoidal density and RBC velocity, respectively. *Bar*: 100 μm. (**B**) and (**C**) Relative changes in sinusoidal diameter and functional sinusoidal density. Data indicate mean ± SE of five to seven separate experiments. (**D**, **E**, and **F**) Alterations in RBC velocity, PO_2, and relative PO_2 recovery in central venules (CV). Data indicate mean ± SE of four to five separate experiments. *Open* and *closed circles* indicate data from hRBC- and α-NO-hRBC-treated groups, respectively. $^*p < 0.05$ as compared with the hRBC-treated control group.

(Panel C) were comparable between the two groups. As seen in Panel D, the recovery of RBC velocity measured at central venules appeared modestly greater in the hRBC-treated group than in the α-NO-hRBC-treated one, but without any statistical significance over the entire course of observation because of the large variation of measurements. Absolute values of PO_2 in central venules were also varied, not only among different rats, but also among individual venules in the same animal, and the measurements indicated no statistical significance (Panel E). However, when the net recovery of PO_2 values was plotted as a function of time after reperfusion, distinct features of local O_2 utilization became evident between the two groups. In the hRBC-treated group, PO_2 values in central venules were abruptly elevated during the initial 5-min period of reperfusion and gradually decreased to the end of observation. On the other hand, those in the α-NO-hRBC-treated group displayed rather slow recovery at the early reperfusion period and reached a plateau level. As a result, the PO_2 in central venules was significantly lower in the α-NO-hRBC-treated group than in the hRBC-treated group during the initial 30-min reperfusion period (Panel F).

We also attempted to measure PO_2 values in portal venules. As seen in Fig. 6A (denoted as P in the panel), it was difficult in rats to find a terminal inlet vessel of portal veins through the surface observation of the liver. Because of this technical difficulty, we were unable to perform accurate PO_2 measurements in the large terminal portal inlets. However, so far as judged from such measurements in periportal regions, including multiple sinusoids adjacent to the terminal portal venules, PO_2 measured at 60 min were approximately 60 mm Hg in the both groups (data not shown). These results collectively suggest that the O_2 consumption occurring between portal and central venules appears to be greater in the α-NO-hRBC-groups than in the hRBC-treated one. Since the intravascular PO_2 determines O_2-saturation rates (SaO_2) of Hb in RBCs, the data indicating periportal and pericentral PO_2 values allow us to estimate the net delivery of O_2 to the hepatic pa-

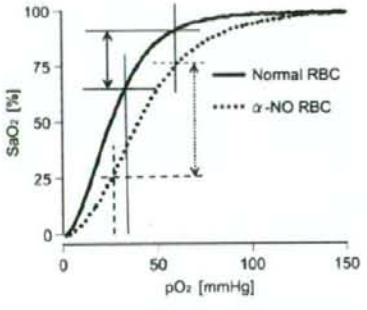

FIG. 7. Differences in oxygen saturation profiles between hRBC (*solid line*) and α-NO-hRBC (*broken line*). *Solid* and *broken arrows* indicate estimations of differences in SaO_2 for hRBC and α-NO-RBC during transition across hepatic microcirculation, respectively. The estimation is based on observations that mean PO_2 values in periportal regions are 70 mm Hg in both groups and those in central venules are 28 and 33 mm Hg in the groups treated with α-NO-hRBC and normal hRBC, respectively (See Fig. 6E).

renchyma and to compare the values between the two groups. Figure 7 illustrates differences in SaO_2 values in periportal and pericentral microvessels between the groups treated with control and α-NO-hRBCs. As demonstrated in previous studies (30, 31), α-nitrosylation of Hb in human RBC caused the right shift of the oxygen saturation curve (dotted line). When mean periportal PO_2 values (60 mm Hg) and those in pericentral venules (33 mm Hg in the normal hRBC and 28 mm Hg in the α-NO-hRBC, as seen in Fig. 6E) of the postischemic livers at 60 min were superimposed on the saturation curves, the net differences in SaO_2 between the portal and central venules were estimated; as seen, the difference for α-NO-hRBC (dotted arrow) was twice greater than that for hRBC (solid arrow). To be noted is that halves of O_2-binding pockets were occupied with NO in α-NO-hRBC. Considering that central RBC velocities did not differ significantly between the two groups (Fig. 6D), these results suggest that α-NO-hRBC and hRBC brings comparable amounts of O_2 to the tissue to the postischemic livers.

DISCUSSION

The present study is the first to examine if administration of RBC with T-state-stabilized Hb by NO pretreatment could improve postischemic dysfunction of peripheral organs such as the liver. Theoretically, T-state stabilization of the Hb allostery does not only enhance oxygen-carrying capacity of RBC to peripheral tissues, but is also believed to lower the threshold to trigger hypoxic vasodilation through delivering NO to microcirculation (19, 24). Such a possible role of Hb allostery in RBC-mediated regulation of organ microvascular function has been considered a mechanism for RBC-dependent delivery of NO under physiologic conditions. However, since R-to-T conversion of the Hb allostery in normal RBC occurs most prominently at specific oxygen tension around 25–30 mm Hg near the P_{50} value (Fig. 1), the theory of Hb-mediated microvascular regulation cannot be applied globally to various organs without actual measurements of local PO_2 and microvascular hemodynamics. A novel laser technology to collect quantitative information of microvascular oxygen delivery has herein allowed us to assess this issue: as seen in results shown in Figs. 1 and 6, the liver is such an organ where α-NO-hRBC could exert its distinct ability to deliver O_2 and to regulate microvascular blood flow.

The current protocols for hypovolemic ischemia induced modest but notable extents of metabolic acidosis concurrently with a significant reduction of the basal bile output, as seen in effects of reperfusion with physiological saline (Fig. 5). Under these circumstances, reperfusion of NO-free hRBC completely repressed the reduction of bile output and induced a recovery of oxygen consumption in the liver parenchyma (Fig. 6E), though a decrease in base excess was not completely recovered. Such effects of hRBC were able to be mimicked by CO-hRBC, suggesting that oxygen delivery by exogenous hRBC is unnecessary to restore the liver function in this particular model. In other words, after shedding 30%–35% of the blood, the rest of rat RBC could function for O_2 delivery in the presence of exogenous hRBC or CO-hRBC. The presence of RBC in circulation does not only contribute to tissue oxygen delivery but also results in an increase in blood viscosity, the factor necessary to maintain wall shear stress to stimulate endothelium-derived vasodilatory mechanisms (1). Considering this fact, improving effects of reperfusion with hRBC on metabolic acidosis and reduced bile output is unlikely to result from its O_2-carrying capacity.

Consideration of the role of O_2-carrying capacity is also useful to determine the superior effects of α-NO-hRBC versus hRBC on the recovery of metabolic acidosis and cholestatic changes in the postischemic liver in the current model. As far as judged from estimated differences in the net drop of SaO_2 versus hepatic microvascular O_2 gradient between portal and central venules (Fig. 7), α-NO-hRBC has the twice greater O_2-carrying capacity than hRBC. However, since 50% of Hb-derived heme of α-NO-hRBC is occupied with NO, the actual amount of oxygen that could be released by this cell in response to the hepatic microvascular O_2 gradient is almost the same as that by NO-free hRBC. If the postischemic recovery of the tissue O_2 consumption is assumed to be identical between the two groups, central PO_2 values in the α-NO-hRBC group should be the same as those in the hRBC group. However, as seen in the data in the early period of reperfusion (Fig. 6), the recovery of central PO_2 in the α-NO-hRBC-treated group was relatively slow, being only 30%–50% of that in the hRBC-treated group. Such a discrepancy in central PO_2 recovery between the estimation and real measurements cannot simply be explained by an insignificant difference in central RBC velocity between the two groups (Panel D in Fig. 6). Assuming that the local oxygen delivery across microvascular beds is diffusion-limited but not flow-limited (28), the current observation allows us to hypothesize that the α-NO-hRBC administration leads to greater recovery of O_2 consumption than in the postischemic liver tissue. Since hepatocytes constitute a major cellular component of the O_2 consumption (23), such a hypothesis is fully supported by our observation that the α-NO-hRBC-treated liver displayed the most notable recovery of the basal bile output, which highly depends on energy-dependent transport of bile salts across hepatocytes (21, 22). Again, the improving effects of α-NO-hRBC seem to be attributable to its greater ability to stimulate O_2 consumption, and are unlikely to result from its distinct ability of O_2-carrying capacity.

Although mechanisms by which the α-NO-hRBC administration results in improved O_2 consumption still remain unknown in the postischemic liver, several possibilities can be considered. First, α-NO-hRBC could deliver more NO to hepatic microcirculation, help cancel superoxide generated upon the early reperfusion period, and attenuate the postischemic damages of hepatocytes that mainly consume oxygen transferred from microcirculation. Such a cancellation of superoxide by endogenous NO could actually be shown to take place in the RBC-free isolated perfused rat liver exposed to anoxia–reperfusion and to help attenuate a reduction of bile output (26, 27). However, several lines of the current experimental data led us to exclude such a hypothesis. The hepatic sinusoids are known to exhibit vasodilation in response to NO or CO through mechanisms involving soluble guanylate cyclase in Ito cells, the liver-specific pericytes (12, 15, 25). However, in liver treated with α-NO-hRBC, central RBC velocity was lower than in that treated with hRBC, despite the absence of difference in sinusoidal diameter during the

whole course of observation (Fig. 6). Furthermore, the delivery of NO from circulation to parenchyma could suppress O_2 consumption in hepatocytes through its ability to inhibit cytochrome oxidase and reduce the basal output (23).

In this context, the second putative mechanism to be considered is involvement of ATP that could also be released from RBC in response to a reduction of local PO_2. Vasoactive responses to extracellularly released ATP are known to differ among different organs (7). In most organs, including intestine and skeletal muscle, extracellular ATP can stimulate purinergic receptors on endothelial cells to increase intracellular calcium ion and stimulate NO production (6). However, the hepatic sinusoid was previously shown to display vasoconstriction by ATP through mechanisms involving Ito cells (12). In addition, hepatocytes can respond to extracellular ATP to stimulate vesicular transport of bile salts and contractility of bile canaliculi and to thereby increase the basal bile output (2, 17, 22). Such tonic actions of ATP on hepatic microvasculature and hepatocytes are obviously supported by oxidative phosphorylation, being in good agreement with our results showing increased O_2 consumption by the α-NO-hRBC-treated postischemic liver. Thus, effects of T-state stabilization on the ability of RBC to excrete ATP in response to reduced PO_2 and identification of purinergic receptors involved in the mechanisms deserve further study and are now underway in our laboratory.

In conclusion, artificial stabilization of T-state Hb by NO is beneficial to protect postischemic liver dysfunction though stimulating O_2 consumption rather than through facilitating the gas delivery. Since the experimental model for hypovolemic hypotension used in the current study gives only modest dysfunction of the liver and never induces shock states, whether the same treatment with T-state-stabilizing RBC is beneficial for treating clinically relevant hemorrhagic shock or irreversible organ injury remains to be examined. However, use of modest severity of the hemorrhagic model seemed suitable to examine the effects of α-NOHb-hRBC on tissue oxygen delivery and consumption in a reliable manner, so far as the protocol for hypotension did not induce heterogeneity in lobular perfusion or any reflow phenomenon and irreversible cell damages that could cause a large variation of O_2 measurements *in vivo*. Biological actions of T-state stabilized RBC on O_2 delivery and consumption deserves further study, given the evidence for its ability to improve hemorrhagic shock or irreversible organ injury.

ACKNOWLEDGMENTS

The authors thank Professor Haruyuki Minamitani for his technical supports to measure PO_2 in hepatic microcirculation. This work was supported by Health Science Research Grants for Research on Advanced Medical Technology from the Ministry of Health, Labor and Welfare in Japan (H17-IYAKU-069), and a grant from New Energy and Industrial Technology Development Organization, Leading Project for Biosimulation from the Ministry of Education and Sciences Technology and Grant-in-Aid for Creative Scientific Research 17GS0419 from JSPS in Japan, and Grant HL14508 from the National Heart, Lung and Blood Institute, the National Institutes of Health, USA.

ABBREVIATIONS

α-NO-hRBC, human red blood cells containing α-nitrosyl Hb; BE, base excess; CO-hRBC, human red blood cells containing COHb; EPR, electron spin resonance; FITC, fluorescein isothiocyanate; HR, heart rate; MAP, mean arterial pressure; Pd-TCPP, Pd-meso-tetra-(4-carboxyphenyl)-porphyrin.

REFERENCES

1. Cabrales P, Tsai AG, and Intaglietta M. Microvascular pressure and functional capillary density in extreme hemodilution with low- and high-viscosity dextran and a low-viscosity Hb-based O_2 carrier. *Am J Physiol Heart Circ Physiol* 287: H363–H373, 2004.
2. Dufour JF, Turner TJ, and Arias IM. Nitric oxide blocks bile canalicular contraction by inhibiting inositol triphosphate-dependent calcium mobilization. *Gastroenterology* 108: 841–849, 1995.
3. Ellsworth ML, Forrester T, Ellis CG, and Dietrich HH. The erythrocyte as a regulator of vascular tone. *Am J Physiol Heart Circ Physiol* 269: H2155–H2161, 1995.
4. Goda N, Suzuki K, Naito M, Tsuchida E, Ishimura Y, Tamatani T, and Suematsu M. Distribution of heme oxygenase isoforms in rat liver: Topographic basis for carbon monoxide-mediated microvascular relaxation. *J Clin Invest* 101; 604–610, 1998.
5. Gladwin MT, Ognibene FP, Pannell LK, Nichols JS, Pease–Fye ME, Shelhamer JH, and Schechter AN. Relative role of heme nitrosylation and beta-cysteine 93 nitrosation in the transport and metabolism of nitric oxide by hemoglobin in the human circulation. *Proc Natl Acad Sci USA* 97: 9943–9948, 2000.
6. Gonzalez–Alonso J, Olsen DB, and Saltin B. Erythrocyte and the regulation of human skeletal muscle blood flow and oxygen delivery. *Circ Res* 91: 1046–1055, 2002.
7. Harrington LS and Mitchell J. Novel role for P2X receptor activation in endothelium-dependent vasodilation. *Br J Pharmacol* 143; 611–617, 2004.
8. Ishikawa M, Sekizuka E, Shimizu K, Yamaguchi N, and Kawase T. Measurement of RBC velocities in the rat pial arteries with an image-intensified high-speed video camera system. *Microvasc Res* 56: 166–172, 1998.
9. Jagger JE, Bateman RM, Ellsworth ML, and Ellis CG. Role of erythrocyte in regulating local O_2 delivery mediated by hemoglobin oxygenation. *Am J Physiol Heart Circ Physiol* 280: H2833–H2839, 2001.
10. Jia L, Bonaventura C, Bonaventura J, and Stamler JS. *S*-nitrosohemoglobin: a dynamic activity of blood involved in vascular control. *Nature* 380: 221–226, 1996.
11. Kajimura M, Shimoyama M, Tsuyama S, Suzuki T, Shunji K, Takenaka S, Tsubota K, Oguchi Y, and Suematsu M. Visualization of gaseous monoxide reception by soluble guanylate cyclase in the retina. *FASEB J* 17: 506–508, 2003
12. Kawada N, Tran–Thi TA, and Decker K. The contraction of hepatic stellate (Ito) cells stimulated with vasoactive substances: possible involvement of endothelin 1 and nitric oxide in the regulation of the sinusoidal tonus. *Eur J Biochem* 13: 815–823, 1993.

13. Kyokane T, Norimizu S, Taniai H, Yamaguchi T, Takeoka S, Tsuchida E, Naito M, Nimura Y, Ishimura Y, and Suematsu M. Carbon monoxide from heme catabolism protects against hepatobiliary dysfunction in endotoxin-treated rat liver. *Gastroenterology* 120: 1227–1240, 2001.
14. Lundberg JO and Weitzberg E. NO generation from nitrite and its role in vascular control. *Arterioscler Thromb Vasc Biol* 25: 1–8, 2005.
15. Makino N, Suematsu M, Sugiura Y, Morikawa H, Shiomi S, Goda N, Sano T, Nimura Y, Sugimachi K, and Ishimura Y. Altered expression of heme oxygenase-1 in the livers of patients with portal hypertensive diseases. *Hepatology* 33: 32–42, 2001.
16. Morisaki H, Katayama T, Kotake Y, Ito M, Ishimura Y, Takeda J, and Suematsu M. Roles of carbon monoxide in leukocyte and platelet dynamics in rat mesentery during sevoflurane anesthesia. *Anesthesiology* 95:192–199, 2001.
17. Nishida T, Gatmaitan Z, Che M, and Arias IM. Rat liver canalicular membrane vesicles contain an ATP-dependent bile acid transport system. *Proc Natl Acad Sci USA* 88: 6590–6594, 1991.
18. Norimizu S, Kudo A, Kajimura M, Ishikawa K, Taniai H, Yamaguchi T, Fujii K, Arii S, Nimura Y, and Suematsu M. Carbon monoxide stimulates mrp2-dependent excretion of bilirubin-IXα into bile in the perfused rat liver. *Antioxid Redox Signal* 5: 449–456, 2003.
19. Pawloski JR, Hess DT, and Stamler JS. Export by red blood cells of nitric oxide bioactivity. *Nature* 409: 622–626, 2001.
20. Rumsey WL, Vanderlooi JM, and Wilson DF. Imaging of phosphorescence: a novel method for measuring oxygen distribution in perfused tissue. *Science* 241: 1649–1651, 1988.
21. Sano T, Shiomi M, Wakabayashi Y, Shinoda Y, Goda N, Yamaguchi T, Nimura Y, Ishimura Y, and Suematsu M. Endogenous carbon monoxide suppression stimulates bile acid-dependent biliary transport in perfused rat liver. *Am J Physiol* 272: G1268–1275, 1997.
22. Shinoda Y, Suematsu M, Wakabayashi Y, Suzuki T, Goda N, Saito S, Yamaguchi T, and Ishimura Y. Carbon monoxide as a regulator of bile canalicular contractility in cultured rat hepatocytes. *Hepatology* 28: 286–295, 1998.
23. Shiomi M, Wakabayashi Y, Sano T, Shinoda Y, Nimura Y, Ishimura Y, and Suematsu M. Nitric oxide suppression reversibly attenuates mitochondrial dysfunction and cholestasis in endotoxemic rat liver. *Hepatology* 27: 108–115, 1998.
24. Stamler JS, Jia L, Eu JP, McMahon TJ, Demchenko IT, Bonaventura J, Gernert K, and Piantadosi CA. Blood flow regulation by *S*-nitrosohemoglobin in the physiological oxygen gradient. *Science* 276: 2034–2037, 1997.
25. Suematsu M, Goda N, Sano T, Kashiwagi S, Shinoda Y, and Ishimura Y. Carbon monoxide: an endogenous modulator of sinusoidal tone in the perfused rat liver. *J Clin Invest* 96: 2431–2437, 1995.
26. Suematsu M, Suganuma K, and Kashiwagi S. Mechanistic probing of gaseous signal transduction in microcirculation. *Antioxid Redox Signal* 5: 485–492, 2003.
27. Taniai H, Suematsu M, Suzuki T, Hori R, Ishimura Y, and Nimura Y. Protective roles of endothelin B receptor-mediated nitric oxide generation in hepatobiliary dysfunction in anoxia-reoxygenated perfused rat liver. *Hepatology* 33: 894–901, 2001.
28. Tsai AG, Johnson PC, and Intaglietta M. Oxygen gradient in microcirculation. *Physiol Rev* 83: 933–963, 2002.
29. Tsukada K, Sekizuka E, Oshio C, Tsujioka K, and Minamitani H. Red blood cell velocity and oxygen tension measurement in cerebral microvessels by double-wavelength photoexcitation. *J Appl Physiol* 96: 1561–1568, 2004.
30. Tsuneshige A and Yonetani T. A novel blood transfusant candidate: intact human erythrocytes containing hemoglobin exclusively nitrosylated in the alpha subunits. *Adv Exp Med Biol* 510: 93–99, 2003.
31. Yonetani T, Tsuneshige A, Zhou Y, and Chen X. Electron paramagnetic resonance and oxygen binding studies of α-nitrosyl hemoglobin. *J Biol Chem* 273: 20323–20333, 1998.

Address reprint requests to:
Makoto Suematsu, M.D., Ph.D.
Professor and Chair
Department of Biochemistry and Integrative Medical Biology
School of Medicine, Keio University
35 Shinanomachi, Shinjuku-ku
Tokyo 160–8582, Japan

E-mail: msuem@sc.itc.keio.ac.jp

Date of first submission to ARS Central, April 1, 2006; date of acceptance, April 14, 2006.

特集　メタボロミクス：包括的代謝物質解析の医学・バイオサイエンスへの応用

メタボローム解析技術による新しい代謝制御機構の系統的探索：ガスバイオロジーの推進と医学への応用

Biomedical Application of Metabolomics

末松 誠　菱木貴子　岩渕拓也　山本雄広　行武良哲　塚田孝祐

Makoto Suematsu, Takako Hishiki, Takuya Iwabuchi, Takehiro Yamamoto, Yoshinori Yukutake, Kosuke Tsukada

CE-MS，あるいはLC-MS/MSを用いた低分子代謝物の網羅的解析法は，データベースに記載されている既存の代謝物のうち特定の疾患で増加するいわゆる疾患マーカーの探索に役立つばかりではなく，未知の代謝物とその代謝経路の同定にも威力を発揮しつつある．筆者らの研究室では，結核菌のような病原微生物の新規クエン酸回路の同定と疾患制御ポイントの探索を行う一方，肝臓におけるチオールの低下の際に増加して，血液中のマーカーとして放出されるオフタルミン酸のようなマーカー分子とその代謝経路の同定を行ってきた．筆者らは生体のストレス応答で増加する一酸化炭素（CO）の標的タンパク質の系統的探索を進めている．

key words

メタボロミクス，含硫アミノ酸，CO，ガスバイオロジー

[1] 末松 誠　慶應義塾大学医学部 医化学教室　E-mail：msuam@sc.itc.keio.ac.jp　URL：http://www.gasbiology.com/

1983年慶應義塾大学医学部卒業，同内科学教室，1991年カリフォルニア大学応用生体医工学部に留学，2001年より現所属，教授．

菱木貴子，岩渕拓也，山本雄広，行武良哲，塚田孝祐　慶應義塾大学医学部 医化学教室

はじめに：メタボロミクスは単なる“網羅的代謝解析”ではない

メタボロミクスを通して得られる網羅的代謝情報は，ゲノミクス情報あるいはプロテオミクス情報との有機的融合によって生物学的にきわめて有用な“生きた情報”として利用できる．図1はコーネル大学微生物学教室のNathan教授との共同研究で，結核菌の解糖系，TCA回路の代謝物の解析を行い，この細菌に特異的なエネルギー代謝経路を見いだした例である[1]．細菌類のTCA回路は基本形はほぼ同じであるが，各酵素反応ステップの活性を比較すると大腸菌と結核菌には大きな違いがあることが判明した．すなわち結核菌ではスクシニルCoAの検出ができず，酵素活性としてのα-ケトグルタル酸デヒドロゲナーゼ（α-KgDH）が欠損していることがわかった．この知見は1962年に別の研究者らが報告しており，結核菌は増殖期にはTCA回路の上半分とグリオキシル酸経路を使って有機酸の代謝を進めると考えられ，広く教科書の記載として認められてきた．しかし，筆者らのLC-MS/MSを利用した解析によれば増殖期にある結核菌の代謝物はコハク酸やグルタミン酸が爆発的に増加することが明らかになり，上記の考え方に疑問が生じた．そこで細菌のα-*KgDH*遺伝子に比較的配列の似た遺伝子産物をいくつか精製し，α-kgを添加してこれが分解されるかどうかを解析すると，ゲノムアノテーションでRv1248cと命名された遺伝子産物がα-Kgデカルボキシラーゼ活性を有すること，生成物としてコハク酸セミアルデヒド（succinic semialdehyde；SSA）ができることが^{1}H-NMRを用いた構造解析により明らかになった．Nathanのグループは同様の手法によってSSAはGabD1/D2遺伝子の産物である酵素によってSSAをコハク酸に変換することも合わせ明らかにし，増殖期の結核菌はα-KgからSSAに迂回してコハク酸に戻す異型TCA回路を持つことが明らかになった（図2）．

このようなKgDHの欠損，Kgを基質としてヒトにはない特異的代謝経路に導くKgデカルボキシラーゼ（図2：Kgd）などの探索は，ゲノミクス情報とメタボローム情報を組み合わせることにより遺伝子発現情報と実際の代謝物プロファイリングによって初めて明らかにされたものである[2]．この酵素はヒトには存在しないため，その阻害剤は治療薬開発の分子標的となる可能性がある．また，結核菌は完全細胞内寄生体であるため，例えばマクロファージに寄生した場合に宿主のα-Kgを奪うことにより，NAPDHオキシダーゼや誘導型NO合成酵素など感染防御に必要なヘム酵素の補欠分子の合成原料となるスクシニルCoAを枯渇させて防御システムの破綻を起こす可能性がないかがさらに検討されるべきであろう．

Ⅰ．ストレス誘導性ガス分子であるCOの標的分子探索

ガス分子は究極の極小分子であり，自身を受容する生体高分子を探索し，吊り上げることは技術的に困難である．筆者らは十数年前に肝臓で生成されるガスである一酸化炭素（CO）が類洞血管を恒常的に拡張し，この臓器の血管抵抗を低く保ち血流を維持することに寄与していることを見いだした[2),3)]．COはヘムオキシゲナーゼ（HO）を介した酸素添加反応によりプロトヘムⅨが分解し，ビリベルジンⅨαと

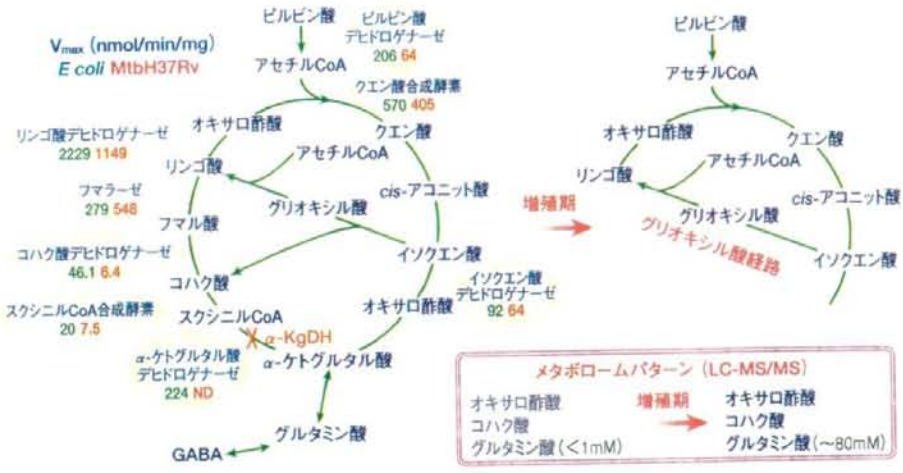

図1. 結核菌と大腸菌のTCA回路の反応ステップごとに酵素活性の比較

左図の緑（大腸菌）と赤（結核菌）の数字はそれぞれの酵素活性（nmol/min/mg タンパク質）を示す．右は1962年にMurthyらによって提唱されたグリオキシル酸経路によるTCA回路の上半分を用いた有機酸代謝経路の考え方．この考え方に従うと，LC-MS/MSにより検出される代謝物プロファイリングの情報と明らかに乖離が生じることから，下半分の回路に新規経路がある可能性が考えられた．

Tian J, et al: Proc Natl Acad Sci USA (2005) 102: 10670-10675より改変．

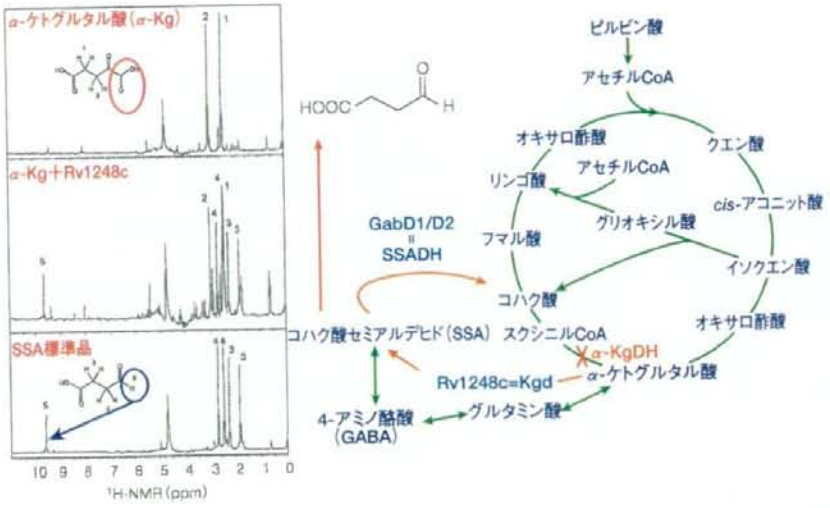

図2. α-ケトグルタル酸デカルボキシラーゼおよびSSADHにより構成される結核菌の異型TCA回路の同定

遺伝子Rv1248cの産物はα-ケトグルタル酸を添加するとカルボキシル基を分解し，新たな水素が現れ，SSAが生成する過程が¹H-NMRにより明らかにされた．Tian J, et al: Proc Natl Acad Sci USA (2005) 102: 10670-10675より改変．

ともに生成するガス分子である．HOは基質であるヘムが酵素に結合すると，それ自身が酵素活性中心を形成して反応が進む珍しい酵素であり，2つのアイソザイム：誘導型のHO-1と構成型のHO-2の存在が知られている．遊離のプロトヘムIXは細胞毒性を有するため，この酵素の生理的ミッションはヘムの解毒であると長く理解されてきたが，COが神経伝達に関与する可能性や肝臓の類洞血管を恒常的に弛緩させる作用があることが報告されて以来[3),4)]，病態時に解毒を実行しつつ，COを介した細胞保護作用を発揮する精妙な生体防御系であることが多くの研究により明らかにされた[5)]（図3）．

肝臓の血管系は入口部にあたる門脈終末枝と中心細静脈の間にはわずか数cmH_2Oの圧較差しか存在しないにもかかわらず豊富な血流を維持している．換言すれば，この臓器には